NeuroImage 61 (2012) 1067–1082

Contents lists available at SciVerse ScienceDirect

NeuroImage

journal homepage: www.elsevier.com/locate/ynimg

An automatic MEG low-frequency source imaging approach for detecting injuries in mild and moderate TBI patients with blast and non-blast causes

Ming-Xiong Huang [a,b,*], Sharon Nichols [c], Ashley Robb [a], Annemarie Angeles [a], Angela Drake [d,1], Martin Holland [d,2], Sarah Asmussen [d], John D'Andrea [a], Won Chun [a], Michael Levy [e], Li Cui [b], Tao Song [b], Dewleen G. Baker [a,f], Paul Hammer [g], Robert McLay [d], Rebecca J. Theilmann [b], Raul Coimbra [h], Mithun Diwakar [b], Cynthia Boyd [d], John Neff [d], Thomas T. Liu [b], Jennifer Webb-Murphy [i], Roxanna Farinpour [d], Catherine Cheung [d], Deborah L. Harrington [a,b], David Heister [b], Roland R. Lee [a,b]

[a] Radiology, Research, Rehab, and Psychiatry Services, VA San Diego Healthcare System, San Diego, CA, USA
[b] Department of Radiology, University of California, San Diego, CA, USA
[c] Department of Neuroscience, University of California, San Diego, CA, USA
[d] Naval Medical Center San Diego, San Diego, CA, USA
[e] Rady Children's Hospital San Diego, University of California, San Diego, CA, USA
[f] Department of Psychiatry, University of California, San Diego, CA, USA
[g] Defense Centers of Excellence for Psychological Health and Traumatic Brain Injury, Arlington, VA, USA
[h] Department of Surgery, University of California, San Diego, CA, USA
[i] Naval Center for Combat and Operational Stress Control, San Diego, CA, USA

ARTICLE INFO

Article history:
Accepted 11 April 2012
Available online 20 April 2012

Keywords:
Magnetoencephalography
Traumatic brain injury
Slow-wave
Blast
Motor vehicle accident
Sport injury

ABSTRACT

Traumatic brain injury (TBI) is a leading cause of sustained impairment in military and civilian populations. However, mild (and some moderate) TBI can be difficult to diagnose because the injuries are often not detectable on conventional MRI or CT. Injured brain tissues in TBI patients generate abnormal low-frequency magnetic activity (ALFMA, peaked at 1–4 Hz) that can be measured and localized by magnetoencephalography (MEG). We developed a new automated MEG low-frequency source imaging method and applied this method in 45 mild TBI (23 from combat-related blasts, and 22 from non-blast causes) and 10 moderate TBI patients (non-blast causes). Seventeen of the patients with mild TBI from blasts had tertiary injuries resulting from the blast. The results show our method detected abnormalities at the rates of 87% for the mild TBI group (blast-induced plus non-blast causes) and 100% for the moderate group. Among the mild TBI patients, the rates of abnormalities were 96% and 77% for the blast and non-blast TBI groups, respectively. The spatial characteristics of abnormal slow-wave generation measured by Z scores in the mild blast TBI group significantly correlated with those in non-blast mild TBI group. Among 96 cortical regions, the likelihood of abnormal slow-wave generation was less in the mild TBI patients with blast than in the mild non-blast TBI patients, suggesting possible protective effects due to the military helmet and armor. Finally, the number of cortical regions that generated abnormal slow-waves correlated significantly with the total post-concussive symptom scores in TBI patients. This study provides a foundation for using MEG low-frequency source imaging to support the clinical diagnosis of TBI.

Published by Elsevier Inc.

Introduction

Traumatic brain injury (TBI) is a leading cause of sustained physical, cognitive, emotional, and behavioral deficits in the civilian population (due to motor vehicle accidents, sports, falls, and assaults) and military personnel (with blast injury as an additional cause). Annually, the Centers for Disease Control reports an estimated 1.7 million people sustain a TBI with 52,000 deaths, 275,000 hospitalizations, and 1.365 million, or nearly 80%, treated and released from an emergency department (Faul et al., 2010). The majority (75%) of the TBIs are in the "mild" range of severity (mTBI) (Centers for Disease Control and Prevention and National Center for Injury Prevention and Control, 2003). An estimated 5.3 million Americans live with disabilities associated with a TBI (Thurman et al., 1999). Blast-related TBI also represents one of the most significant health issues among surviving soldiers wounded in combat in Iraq and Afghanistan. These individuals often have residual impairments which have been attributed to central nervous system (CNS) damage either

* Corresponding author at: Radiology Imaging Laboratory, University of California at San Diego, 3510 Dunhill Street, San Diego, CA 92121, USA. Fax: +1 858 534 6046.
E-mail address: mxhuang@ucsd.edu (M.-X. Huang).
[1] Current Institute: Dynamics Research Corporation, Vienna, VA, USA.
[2] Current Institute: Trinity Mother Frances Neuroscience Institute, Tyler, TX, USA.

1053-8119/$ – see front matter. Published by Elsevier Inc.
doi:10.1016/j.neuroimage.2012.04.029

as a direct result of the blast (e.g., blast-wave concussion or blunt trauma from impact) or as a secondary effect of damage to other organs such as the lungs.

Although post-concussive symptoms (PCS) in mTBI often resolve by three months after injury in the majority of individuals (Levin et al., 1987; Rutherford, 1989), about 20% (varying from 8 to 33%) of mTBI patients show persistent long-term cognitive and/or behavioral impairments (Alexander, 1995; Binder, 1986, 1997; Bohnen et al., 1992; Rimel et al., 1981; Rutherford, 1989). There have been few effective treatments for mTBI. Conventional neuroimaging techniques have limited sensitivity to detect physiological alterations caused by TBI and are usually not used to assess the efficacy of mTBI treatments. Mild (and some moderate) TBI can be difficult to detect because the injuries are often not visible on conventional acute MRI or CT (Bigler and Orrison, 2004; Johnston et al., 2001; Kirkwood et al., 2006). Approximately 80% of civilian patients with TBI do not show visible lesions using conventional MRI or CT (Alexander, 1995). For mTBI, intracranial lesions were detected with conventional neuroimaging techniques in only 4%, 16%, and 28% of patients with Glasgow Coma Scale scores (Teasdale and Jennett, 1974) of 15, 14, and 13, respectively (Culotta et al., 1996). Similarly, closed-brain injuries outnumbered penetrating injuries in more than 450 U.S. military TBI patients injured in Iraq and treated as inpatients between January 2003 and February 2007 at Walter Reed Army Medical Center. Of these closed-brain injuries, 56% were considered moderate or severe, and 44% were mild, with no visible lesion on clinical MRI or CT (Okie, 2005). A more recent combat-related TBI study in Operation Iraqi Freedom with 2074 participants showed that 89% of all TBIs were mild (MacGregor et al., 2010). The diagnosis of combat-related mTBI is based primarily on the characteristics of the acute clinical sequelae, following the injury and lesion(s) may be "subtle, scattered, varied,…, not detected on conventional brain CT" (Van Boven et al., 2009). These examples illustrate the limited diagnostic utility of standard neuroimaging techniques in this population. Furthermore, the absence of abnormalities on conventional neuroimaging techniques in the majority of mTBI patients even with post-concussive symptoms and cognitive and/or behavioral deficits illustrates the limited prognostic value of conventional neuroimaging techniques.

Usually, PCS and cognitive deficits in TBI patients cannot be explained solely by focal pathology; traumatic axonal injury (TAI) is another major contributor to these deficits. TAI is commonly induced by a sudden acceleration–deceleration or rotational forces. In a rodent TBI model, a silver staining technique reveals that axonal injury was the most prominent feature following blast exposure (Garman et al., 2011). In humans, the subsequent tissue injury is characterized by axonal stretching, inflammation, disruption, and separation of nerve fibers, although axotomy has been found to be relatively rare in even severe TBI (Adams et al., 1989; Basser and Pierpaoli, 1996; Gennarelli et al., 1982; Xu et al., 2007). Conventional CT and MRI are primarily sensitive to blood from nearby torn capillaries, and less sensitive to axonal damage itself, hence they underestimate the presence of TAI, especially in mTBI cases. The limited diagnostic value and poor predictive utility for long-term outcome of the conventional neuroimaging techniques underscore the urgent need for new neuroimaging methods for better diagnosis and longitudinal assessment of mTBI. The availability of neuroimaging techniques with greater sensitivity to the physiological alterations caused by TBI could promote the development of treatment interventions for mTBI through an improved understanding of brain mechanisms of injury.

Diffusion tensor imaging (DTI)

Diffusion tensor imaging (DTI) measures white-matter integrity in the brain by measuring the Brownian motion of water through tissues. Information obtained from DTI is representative of the local physical properties of tissue and may be used to estimate the location and orientation of white matter within the brain. Recently, DTI has also been used to examine potential axonal injury in mTBI patients with promising results. DTI has been successfully applied in mild, moderate, and severe TBI (Arfanakis et al., 2002; Gupta et al., 2005; Huisman et al., 2004; Inglese et al., 2005; Lee et al., 2006; Salmond et al., 2006; Xu et al., 2007), and the method has shown great potential in providing a better understanding and improved diagnosis of TAI. DTI studies in TBI patients have reported reduced fractional anisotropy (FA) in major white-matter tracts in central areas of the brain (Arfanakis et al., 2002; Gupta et al., 2005; Inglese et al., 2005; Salmond et al., 2006; Wilde et al., 2006; Xu et al., 2007), and the FA abnormality correlates with the GCS and post-traumatic amnesia (Benson et al., 2007). In mTBI patients (civilians and blast-injured military personnel), reduced FA values were found in anterior corona radiata, uncinate fasciculus, corpus callosum, inferior and superior longitudinal fasciculus, cingulum bundle, and middle cerebellar peduncles (Davenport et al., 2012; Mac Donald et al., 2011; Miles et al., 2008; Niogi et al., 2008; Rutgers et al., 2008; Smits et al., 2011). FA reduction is attributed to a change in the parenchymal structure, which may include misalignment of fibers, edema, fiber disruption, and axonal degeneration (Niogi et al., 2008; Rutgers et al., 2008). We also reported reduced FA in a multimodal MEG-DTI study of mTBI (Huang et al., 2009). However, increased FA (Bazarian et al., 2007; Henry et al., 2011; Mayer et al., 2011; Wilde et al., 2008) or no change in FA (Messe et al., 2011; Zhang et al., 2010) has also been reported in mTBI, indicating that more research is needed to delineate the relationships between DTI parameters and underlying neuropathological processes in mTBI.

With these considerations in mind, the present study examined the sensitivity of a new magnetoencephalography (MEG) source imaging approach for detecting pathology in mTBI. MEG demonstrates sensitivity to abnormal neuronal signals resulting from axonal injuries. Pioneering studies by Lewine and colleagues showed that the brains of mTBI patients generate abnormal low-frequency magnetic fields that can be measured and localized by MEG (Lewine et al., 1999; Lewine et al., 2007). They also showed that MEG was more sensitive than conventional MRI or EEG for detecting abnormalities in mTBI patients. Unlike normal spontaneous MEG data which is dominated by neuronal activity with frequencies above 8 Hz, injured neuronal tissues (due to head trauma, brain tumors, stroke, etc.) generate abnormal focal or multi-focal low-frequency neuronal magnetic signal (delta-band 1–4 Hz, or theta-band 5–7 Hz) that can be directly measured and localized using MEG (Baayen et al., 2003; de Jongh et al., 2003; Decker and Knott, 1972; Lewine and Orrison, 1995; Lewine et al., 1999; Nagata et al., 1985; Vieth et al., 1996). However, to make MEG low-frequency source imaging an effective clinical tool for assisting in the diagnosis of mTBI, one must address the following two key questions: 1) what is the neuronal mechanism of abnormal MEG slow-waves in TBI and how are the slow-waves related to axonal injuries? 2) Is it possible to develop an objective, automated, and operator-independent MEG low-frequency source imaging method for detecting and localizing the MEG slow-waves? The first question was addressed by our recent mTBI study using MEG and diffusion tensor imaging (DTI) (Huang et al., 2009), which examined the relationship between DTI abnormalities in white-matter fiber tracts and the generation of abnormal MEG slow-waves in mTBI. To appreciate the relationship between MEG slow-wave and DTI findings in mTBI, it is important to review the closely related animal studies.

Animal studies of delta-wave generation in gray matter and axonal injuries in white matter

Neurophysiological studies in animals have established a solid connection between pathological delta-wave generation in gray

matter and axonal injuries in white matter. Gloor, Ball, and colleagues showed that polymorphic delta-band slow-waves produced by white-matter axonal lesions in the cat are localized to the area of cortex overlying the lesion (Gloor et al., 1977). They performed a series of experiments using a combination of cortical surface electrodes, microelectrodes, and depth electrodes to identify the generators of the delta-waves and establish their relationship to single cell discharge of cortical neurons (Ball et al., 1977; Gloor et al., 1977). They found that delta-waves due to white-matter lesion formation by thermocoagulation were predominantly generated in pyramidal neurons of layer V or its vicinity, overlying the axonal lesion in white matter. They also found that delta-waves can be induced by the administration of atropine to block the afferent axonal input (Schaul et al., 1978). These experiments concluded that partial cortical *de-afferentation* was an important factor in delta-wave production. Our human MEG-DTI results were compatible with this conclusion, showing that MEG delta-waves in TBI patients are generated from gray-matter neurons that experience de-afferentation due to axonal injury in the underlying white-matter fiber tracts (Huang et al., 2009).

Currently, MEG slow-wave detection and localization are usually manually performed by MEG analysts. We are not aware of any standards for MEG slow-wave analysis in mTBI. The lack of objective approaches makes it difficult to compare results across different operators and MEG centers. In the present study, we address this obstacle for making MEG low-frequency source imaging an effective tool for assisting in the diagnosis of mTBI. There are several goals for this study: 1) design a new automated and operator-independent MEG source imaging approach and establish a normative database for identifying and localizing abnormal slow-waves in TBI patients. 2) Examine the sensitivity of the new approach for assisting with the diagnosis of mTBI (due to blast and non-blast causes) and moderate TBI patients. 3) Identify common and distinct features of the abnormal MEG slow-wave generation in 96 cortical gray-matter regions (i.e., from Harvard–Oxford Gray-matter Atlas in MNI-152 space) among different TBI patient groups. 4) Correlate findings from our new MEG slow-wave source imaging method with patients' symptoms.

Materials and methods

Theory of frequency-domain VESTAL source imaging for oscillatory MEG signal

MEG signals in time and frequency domains

First, we take an imaging (lead-field) approach and divide the source space (gray-matter brain volume) into a grid of source locations. MEG time-domain signal can then be expressed in a data matrix: $\mathbf{B}(t)=[\mathbf{b}(t_1),\mathbf{b}(t_2),\ldots,\mathbf{b}(t_N)]$, where N is the number of time samples and $\mathbf{b}(t_i)$ is a $M\times 1$ vector containing the magnetic fields at M sensor sites at time point t_i. The data matrix can be expressed as:

$$\mathbf{B}(t)=\mathbf{G}\mathbf{Q}(t)+\mathbf{Noise}(t) \tag{1}$$

where $\mathbf{G}$ is an $M\times 2P$ gain (lead-field) matrix calculated from MEG forward modeling for the pre-defined source grid with P dipole locations, with each dipole location having two orthogonal orientations (i.e., $\boldsymbol{\theta}$ and $\boldsymbol{\phi}$). The $\mathbf{Q}(t)$ is a $2P\times N$ source time-course matrix. In the spherical MEG forward head model, $\boldsymbol{\theta}$ and $\boldsymbol{\phi}$ represent the two tangential orientations for each dipole location, whereas in a realistic MEG forward model using the boundary element method (BEM), the $\boldsymbol{\theta}$ and $\boldsymbol{\phi}$ orientations are obtained as the two dominant orientations from the singular value decomposition (SVD) of the $M\times 3$ lead-field matrix for each dipole, as previously documented (Huang et al., 2006). The inverse solution in Eq. (1) is to obtain the source time-courses $\mathbf{Q}(t)$ for given MEG sensor wave-forms $\mathbf{B}(t)$. In general, for each time-sample, since the number of unknown parameters is far greater than the number of sensor measurements (i.e. $2P\gg M$), MEG source imaging is dealing with a highly under-determined problem, and there are a large number of solutions that will fit the data. To reduce the ambiguity, additional constraints (source models) are needed.

VEctor-based Spatio-Temporal analysis using L1-minimum norm (VESTAL) is a high-resolution time-domain MEG source imaging solution for Eq. (1) (Huang et al., 2006) with the following properties: 1) can model many dipolar and non-dipolar sources; 2) requires no pre-determination of the number of sources (model order); and 3) can resolve 100% temporally correlated sources (Brang et al., 2010; Huang et al., 2006; Huang et al., 2010). To more effectively image oscillatory MEG signals such as complicated MEG slow-waves, we expand VESTAL from time-domain to frequency-domain. By doing this, we only need to analyze the MEG signal for a few frequency bins instead of thousands of time samples in a given time window (e.g., an epoch). To image resting-state MEG signal, we first divide the spontaneous time-domain data into epochs. By performing Fast Fourier Transform (FFT) to transfer each epoch into F frequency bins, Eq. (1) becomes:

$$\left[\mathbf{K}_{real}(f)\quad \mathbf{K}_{imag}(f)\right]=\mathbf{G}\left[\boldsymbol{\Omega}_{real}(f)\quad \boldsymbol{\Omega}_{imag}(f)\right] \tag{2}$$

where the $M\times F$ matrices $\mathbf{K}_{real}$ and $\mathbf{K}_{imag}$ are the real and imaginary parts of the FFT of the sensor waveform $\mathbf{B}(t)$ for given frequency f, and $2P\times F$ matrices $\boldsymbol{\Omega}_{real}$ and $\boldsymbol{\Omega}_{imag}$ contain the Fourier Transformation coefficients of source time-course $\mathbf{Q}(t)$. The inverse solution to the frequency-domain Eq. (2) is to find $\boldsymbol{\Omega}_{real}$ and $\boldsymbol{\Omega}_{imag}$ which are the source amplitudes at different frequency bins, for given sensor-space frequency-domain signal $\mathbf{K}_{real}$ and $\mathbf{K}_{imag}$. As in the time-domain, such an inverse problem is under-determined.

Frequency-domain L1-minimum norm solution

Letting $\boldsymbol{\omega}$ be the $2P\times 1$ source-spaced Fourier coefficient vector from a column in either $\boldsymbol{\Omega}_{real}$ or $\boldsymbol{\Omega}_{imag}$ for a given frequency bin (we will drop the "real" and "imag" subscripts for now), and letting $\mathbf{G}=\mathbf{U}\mathbf{S}\mathbf{V}^T$ be the truncated singular value decomposition of the gain matrix, the L1-minimum norm solution to Eq. (2) will be:

$$\min\left(\mathbf{w}^T|\boldsymbol{\omega}|\right),\ \text{subject to constraints}\ \ \mathbf{S}\mathbf{V}^{\mathbf{T}}\boldsymbol{\omega}\cong\mathbf{U}^{\mathbf{T}}\boldsymbol{\kappa} \tag{3}$$

where $\boldsymbol{\kappa}$ is the sensor-spaced Fourier coefficient vector from the corresponding column in either $\mathbf{K}_{real}$ or $\mathbf{K}_{imag}$. For VectorView™ MEG system (Elekta/Neuromag, Helsinki, Finland), we keep the top 40 singular values during the SVD truncation of the gain matrix $\mathbf{G}$. In Eq. (3), $\mathbf{w}$ is a $2P\times 1$ weighting vector chosen to remove potential bias towards grid nodes at the superficial layer and it is usually taken to be the column norm of the $\mathbf{G}$ matrix (Huang et al., 2006; Matsuura and Okabe, 1997; Uutela et al., 1999) or a Gaussian function (Ioannides et al., 1993). In general, the solution to Eq. (3) is a non-linear minimization procedure since the source-space Fourier coefficient $\boldsymbol{\omega}$ can be either positive or negative. However, in practice, one can always replace the absolute values in $|\boldsymbol{\omega}|$ with the following two sets of non-negative values related to $\boldsymbol{\omega}$, and solve the set of equations through linear programming (LP): with the introduction of two new non-negative variables $\boldsymbol{\omega}^a$ and $\boldsymbol{\omega}^b$ (Eiselt et al., 1987), we can re-write Eq. (3) as:

$$\begin{aligned}&\min\left(\mathbf{w}^T\left(\boldsymbol{\omega}^a+\boldsymbol{\omega}^b\right)\right)\ \text{s.t.}\mathbf{S}\mathbf{V}^{\mathbf{T}}\boldsymbol{\omega}\cong\mathbf{U}^{\mathbf{T}}\boldsymbol{\kappa},\\ &\boldsymbol{\omega}=\boldsymbol{\omega}^a-\boldsymbol{\omega}^b,\left\{\omega_j^a\right\},\left\{\omega_j^b\right\}\geq 0,\left\{\omega_j\right\},j=1,2,\ldots,2P.\end{aligned} \tag{4}$$

Eq. (4) can be readily solved by several LP packages. In this study, SeDuMi (http://sedumi.ie.lehigh.edu/) is used to solve the above equation-set to get source imaging $\boldsymbol{\omega}$ for a given frequency bin. This step is repeated for each frequency bin to obtain the whole

frequency-domain source images for both the real and imaginary parts of the signal, i.e. $\mathbf{\Omega}_{real}$ or $\mathbf{\Omega}_{imag}$.

One problem that needs to be addressed by the minimum L1-norm approach is that the solution has a small tendency (bias) towards the coordinate axes. For example, in spherical MEG head model, for a dipole at the ith node of the grid, the vector-based L1-minimum norm solution can also be expressed as minimizing $\sum_{i=1}^{P} w_i\omega_i(|\cos(\psi_i)| + |\sin(\psi_i)|)$ where ψ_i is the angle between the total dipole moment and the orientation of the elevation in a tangential plane containing the dipole node, and $\omega_i = \sqrt{(\omega_i^{\theta})^2 + (\omega_i^{\varphi})^2}$ is the non-negative dipole strength. This will introduce a bias towards the coordinate axes (Fig. 1 in Huang et al., 2006). In order to handle this small bias, an additional correction factor $(|\cos(\psi_i^e)| + |\sin(\psi_i^e)|)^{-1}$ was included in the weighting vector $\boldsymbol{w}$ in Eq. (4) for one more iteration, where ψ_i^e is the angle associated with the estimated orientation based on L1-minimum norm solution without the correction factor.

Frequency-domain VESTAL

One major problem of the conventional time-domain L1-norm approaches is its instability in spatial construction and discontinuity in reconstructed source time-courses. This is commonly seen as "jumps" from one grid point to (usually) the neighboring grid points. Equivalently, the time-course of one specific grid point can show substantial "spiky-looking" discontinuity. Direct frequency-domain L1-norm solution (i.e. $\mathbf{\Omega}_{real}$ or $\mathbf{\Omega}_{imag}$) operating on individual frequency bins will also suffer from the same instability as the conventional approaches. In the time-domain, we previously developed VEctor-based Spatio-Temporal Analysis using L1-minimum norm (VESTAL), which can drastically increase spatial and temporal stability (Huang et al., 2006). The idea was based on a principle of MEG physics, which states that the magnetic waveforms in the sensor-space are linear functions of the dipole time-courses in the source-space. Here, we introduce a similar approach for frequency-domain VESTAL. In this approach, we perform SVD for the $M \times F$ frequency domain MEG sensor signal (we drop the "real" and "imag" subscripts since it applies to both):

$$\mathbf{K} = \mathbf{U}_B\mathbf{S}_B\mathbf{V}_B^T. \tag{5}$$

One can see that all frequency-related information in the MEG sensor signal can be represented as a linear combination of the singular vectors in the matrix $\mathbf{V}_B$. Since MEG sensor-spaced signals are linear functions of the underlying neuronal source-space signal, the same signal sub-space that expands the frequency dimension of sensor-space Fourier coefficient matrix $\mathbf{K}$ should also expand the frequency dimension of the $2P \times F$ source-space Fourier coefficient matrix $\mathbf{\Omega}$ (we also drop the "real" and "imag" subscripts here). By projecting $\mathbf{\Omega}$ towards $\mathbf{V}_B$ we can ensure that source spectral matrix $\mathbf{\Omega}$ and sensor spectral matrix $\mathbf{K}$ share the same frequency information as required by the MEG physics:

$$\mathbf{\Omega}_{Freq_VESTAL} = \mathbf{\Omega}\mathbf{P}_{||} \tag{6}$$

where the projection matrix $\mathbf{P}_{||} = \mathbf{V}_B\mathbf{V}_B^T$ is constructed using the dominant (signal-related) temporal singular vectors (subspace) of the sensor waveforms. We call $\mathbf{\Omega}_{Freq\_VESTAL}$ the Frequency-domain VESTAL solution. The procedure (Eqs. (4)–(6)) applies to the real and imaginary parts of the signal separately. Later, the frequency-domain VESTAL source image is obtained by combining the real and imaginary parts together.

Research subjects

Forty-five (45) mTBI and ten (10) moderate TBI patients who had a documented sub-acute/chronic TBI (4 weeks to 3 years, mean 8.2 ± 7.1 months post-injury) with persistent ongoing post-concussive symptoms participated in this study. TBI patients were divided into three groups: The mild blast-induced TBI group consisted of 23 mTBI patients (military personnel) with injuries caused by blast exposure during combat (age 26.0 ± 5.3 years, all males) while the mild non-blast TBI group contained 22 mTBI patients injured due to non-blast causes (i.e., motor vehicle accidents, sports, and falls; age 29.1 ± 13.3 years, 15 males). The moderate TBI group consisted of 10 moderate TBI patients (age 29.2 ± 13.2 years, 8 males) whose injuries were not blast-induced, with similar causes as in the mild non-blast TBI group. One essential step in identifying individual TBI patients with abnormal MEG slow-waves is to first create an age-matched normative database (see below). For that purpose, 44 healthy control subjects with no significant history of concussion were recruited in the study (age 26.5 ± 8.0 years, 37 males). There were no statistically significant age differences between the healthy control group and any of the three TBI groups.

All TBI patients were carefully evaluated in a clinical interview to document the nature of the injuries and on-going symptoms. The diagnosis and classification of TBI patients were based on accepted diagnostic criteria. Inclusion in the mTBI patient group required a documented TBI that meets the following criteria: a loss of consciousness (LOC) <30 min or feeling "dazed" or "confused" or "seeing stars" immediately after the trauma, a post-traumatic amnesia (PTA) <24 h, an initial GCS score (Teasdale and Jennett, 1974) between 13 and 15 (if available), and persistent ongoing post-concussive symptoms. The GCS is applied to all civilian patients and to a subset of military personnel with mTBI in whom the scores were available. Since the GCS assessment was often not available in theater, military personnel with missing GCS, but who met the inclusion criteria LOC and PTA, were also recruited. Criteria for inclusion in the moderate *civilian* TBI patient group includes: LOC <24 h, but >30 min, an initial GCS between 9 and 12, a PTA >24 h, but <7 days, and persistent ongoing post-concussive symptoms.

Screening for participants in the active-duty military patients with blast-induced mTBI was done during their intake into Defense and Veterans Brain Injury Center (DVBIC) at Camp Pendleton and Naval Medical Center San Diego (NMCSD). We used all available records in the patient's medical chart as well as patient interview and in some cases, a screening battery of tests. The study was described to patients who met the criteria for study participation and their interest was gauged before a referral was made.

Tertiary injuries were common in mTBI patients with blast cause. Among our 23 blast-induced TBI patients, 17 also reported having tertiary injuries; 3 reported no-tertiary injuries; 3 unsure. The tertiary injuries involved a fall, hitting other objects (e.g., hitting parts of vehicle when the driving vehicle was hit by an IED), or being hit by other flying objects following the initial blast (Cernak and Noble-Haeusslein, 2010; Elder et al., 2010). We use the term "blast-induced" throughout this study to represent the group with combined blast and tertiary injuries. In each TBI group, two patients had positive findings on conventional MRI (nonspecific mild white-matter T2-prolongation, not definitely related to trauma) and none had evidence of intracranial hemorrhage/hemosiderin during the *chronic* phase (i.e., >6 months post-injury). No healthy control subjects showed positive findings on conventional MRI.

We also examined PCS in all 55 TBI patients, which was based on a clinical interview. The symptoms were coded as "1" for existence of symptoms and "0" for absence of symptoms in 21 categories, modified slightly from the Head Injury Symptom Checklist (HISC, McLean et al., 1984) : 1) headaches, 2) dizziness, 3) fatigue, 4) memory difficulty, 5) irritability, lack of patience, lose temper easily 6) anxiety, 7) trouble with sleep, 8) hearing difficulties, 9) blurred vision and other visual difficulties, 10) personality changes (e.g., social problems), 11) apathy, 12) lack of spontaneity, 13) affective lability (quick-changing emotions), 14 depression, 15) trouble concentrating, 16) bothered by

noise, 17) bothered by light, 18) coordination and balance problems, 19) motor difficulty, 20) difficulty with speech, and 21) numbness/tingling.

The focus of the present study is to see whether MEG can detect on-going abnormal loci and networks injured by TBI. It is not our intention in this study to use MEG to distinguish new from old neuronal injuries due to multiple TBIs. Patients with multiple TBIs were allowed, and a history of the most recent and all prior TBIs was documented for further exploration. It is possible that in patients with multiple TBIs, both the old and new injuries may lead to de-afferentation, thus the generation of abnormal MEG slow-waves. The numbers of subjects with multiple TBIs were 3, 5, and 0 for mild blast-induced, mild non-blast, and moderate TBI groups, respectively.

Exclusion criteria in all TBI and healthy control groups included other neurological or psychiatric disorders (e.g., brain tumor, stroke, epilepsy, Alzheimer disease, schizophrenia, and post-traumatic stress disorder (PTSD)); a history of learning disability or ADHD; substance or alcohol abuse according to DSM-IV criteria within the six months prior to the study; history of metabolic or other diseases known to affect the CNS (see Dikmen et al., 1995 for similar criteria); extensive metal dental hardware, or other metal objects in the head, neck, or face areas that cause non-removable artifacts in the MEG data; or currently taking neuroleptic, sedative, or hypnotic medications which may increase activity in delta-frequency. Subjects diagnosed with Major Depression Disorder prior to the TBI were also excluded. However, since depression is a typical clinical symptom after head injury, we documented, but did not exclude the subjects with depression symptoms after the injury. The numbers of patients diagnosed with depression were 5, 4, and 3 for the blast-induced mTBI, non-blast mTBI, and moderate TBI groups, respectively.

MEG data acquisition and signal pre-processing to remove artifacts

Resting-state MEG data (spontaneous recording for detecting low-frequency MEG signals) were collected using the VectorView™ whole-head MEG system (Elekta-Neuromag, Helsinki, Finland) with 306 MEG channels in upright position inside a multi-layer magnetically-shielded room (IMEDCO-AG) (Cohen et al., 2002) at the UCSD MEG Center. The recording was divided into three 5-minute blocks with eyes closed, alternating with three 5-minute blocks with eyes open. In eyes-closed condition, the subject was instructed to keep the eyes closed and empty his/her mind. In eyes-open condition, the subject was instructed to fix the eyes on a fixation point and empty his/her mind. The order of blocks was counter-balanced between subjects. Data were sampled at 1000 Hz and were run through a high-pass filter with 0.1 Hz cut-off and a low-pass filter with 330 Hz cut-off. Eye blinks, eye movements, and heart signals were monitored. Precautions were taken to ensure head stability: foam wedges were inserted between the subject's head and the inside of the unit, and a Velcro strap was placed under the subject's chin and anchored in superior and posterior axes. The head positions were measured and we ensured that the head movement across different sessions was less than 5 mm (usually 2–3 mm). Since the MEG eyes-open data were heavily contaminated with eye-blinks in the majority of the subjects, we focused on analyzing the eyes-closed data in the present study.

MEG eyes-closed data are first run through MaxFilter, also known as signal space separation, (Song et al., 2008; Taulu et al., 2004a, 2004b) to remove external interferences (e.g., magnetic artifacts due to metal objects, strong cardiac signals, environment noises, etc.), and to co-register the MEG data by removing the small head movements across the three 5-min eyes-closed sessions. Next, residual artifacts near the sensor array due to eye movements and residual cardiac signals are removed using Independent Component Analysis. The software is our customized version of ICALAB (*bsp.brain.riken.jp/ICALAB/*).

The EKG artifacts in the MEG data were also removed when the MEG data were passed through MaxFilter. This feature of MaxFilter has been shown in (Song et al., 2008; Taulu et al., 2004a, 2004b). In fact, removing EKG artifacts using MaxFilter was quite straight forward since they are clearly part of magnetic fields in the Vector Spherical Harmonic Expansion (in signal space separation), external to the MEG sensor array.

Structural MRI, MEG-MRI registration, BEM forward calculation

Structural MR images of the subject's head were collected using a General Electric 1.5T Excite MRI scanner (ver. 14 software release). The acquisition contains a standard high-resolution anatomical volume with a resolution of $0.94\times0.94\times1.2$ mm^3 using a T1-weighted 3D-IR-FSPGR pulse sequence. To co-register the MEG with MRI coordinate systems, three anatomical landmarks (i.e., left and right pre-auricular points, and nasion) were measured for each subject using the Probe Position Identification system (Polhemus, USA). By identifying the same three points on the subject's MR images using MRILAB software developed by Elekta/Neuromag, a transformation matrix involving both rotation and translation between the MEG and MR coordinate systems was generated. To increase the reliability of the MEG-MR co-registration, approximately 80 points on the scalp were digitized with the Polhemus system, in addition to the three landmarks, and those points were co-registered onto the scalp surface of the MR images. Based on our experience with MEG median-nerve task that is well-known to produce reliable responses at the primary somatosensory cortex for hand representations that are associated with unique anatomical landmarks (Huang et al., 2000, 2006), the MEG-MR co-registration error is expected to be less than 3 mm. The T1-weighted images were also used to extract the innermost skull surface (SEGLAB software developed by Elekta/Neuromag). The innermost skull surface was used to construct a realistic head model for MEG forward calculation based on Boundary Element Method (BEM) (Huang et al., 2007; Mosher et al., 1999).

In addition to the T1-weighted MRI, the following conventional MRI sequences typical for identifying lesions in TBI patients were performed: 1) Axial T2*-weighted; 2) Axial fast spin-echo T2-weighted; 3) Axial FLAIR; and 4) Axial DWI. These conventional MRIs were carefully reviewed by a Board-certified neuroradiologist (R.R. Lee) to determine if the subject had visible lesions on MRI.

Processing stream of frequency-domain VESTAL source imaging for MEG slow-wave signal

Each of the artifact-free, 5-minute long, eyes-closed, resting-state MEG sensor-space data was run through a band-pass filter with the passing band at 1–4 Hz (delta-frequency band) and transition bands (Hanning Windows) of 0.5–1 Hz and 4–6 Hz, respectively. Then the sensor-space MEG data were divided into 2.5-second epochs with 50% overlap in time. For each epoch, an FFT was performed to obtain the sensor-space FFT coefficients $\mathbf{K}_{real}$ and $\mathbf{K}_{imag}$ for 11 equally-spaced low-frequency bins with center frequencies between 0.98 Hz and 5.86 Hz. These sensor-space frequency-domain data were used by the frequency-domain VESTAL to obtain the MEG low-frequency source images.

The source grid used by Frequency-domain VESTAL was obtained by sampling the gray-matter areas from the T1-weighted MRI of each subject. Fig. 1 illustrates this step: 1) the T1-weighted MR images from a subject (Fig. 1(a)) are registered to a standard atlas (e.g., MNI-152) as in Fig. 1(b) using registration programs in FSL (www.fmrib.ox.ac.uk/fsl/). 2) The cortical (Fig. 1(c)), subcortical, and cerebellum gray-matter masks with pre-defined brain regions from the standard atlas are transferred to the individual subject's coordinates (Fig. 1(d)), using the inverse of the transformation in the first step. The Harvard–Oxford Atlas, as part of the FSL software

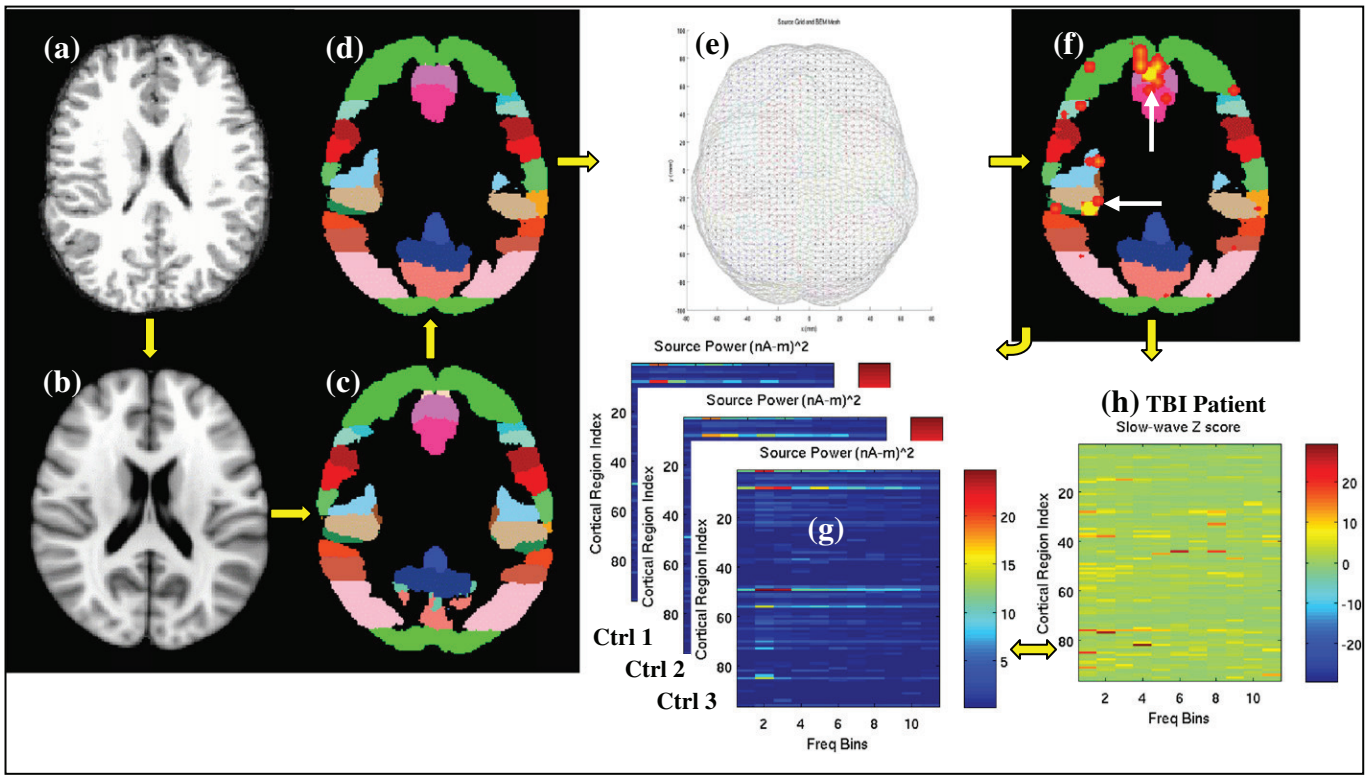

Fig. 1. Processing stream of frequency-domain VESTAL MEG source imaging for slow-wave signal: (a) individual subject's T1-weighted MRI; (b) MNI-152 Brain Atlas; (c) Harvard–Oxford cortical region mask in MNI-152 coordinate; (d) cortical region mask is transferred to the individual subject's MRI coordinate; (e) cortical regions are re-sampled to MEG source grid with a 5-mm grid size for frequency-domain VESTAL. The gray triangles are the BEM mesh; (f) MEG slow-wave activities (hot spots) obtained with frequency-domain VESTAL. Cortical mask is then applied to these slow-wave activities; (g) MEG slow-wave power diagrams (cortical regions versus frequency bins) for healthy control subjects are used to construct normative database; (h) Comparing the slow-wave power from a TBI patient with the normative database, a Z-score diagram is obtained. Increased slow-wave activities are shown in yellow and red color.

with masks of a) 96 cortical gray-matter regions (48 in each hemisphere, see Table 1), b) 15 sub-cortical gray-matter regions, and c) cerebellum, is used in this step. 3) The regional masks in this subject are re-sampled to a cubic source grid with 5 mm in size (Fig. 1(e)) for frequency-domain VESTAL analysis. Note that the color coding for different brain regions in this subplot is different from the one used in Figs. 1(c) and (d). Realistic BEM head model was used for MEG forward calculation, with the BEM mesh obtained from tessellating the inner skull surface from the MRI into ~6000 triangular elements with ~5 mm in size shown as the gray triangles in Fig. 1(e).

Frequency-domain VESTAL analysis (i.e., Eqs. (4)–(6)) was performed for the real and imaginary part of each epoch separately to obtain the frequency-domain source imaging $\mathbf{\Omega}_{Freq\_VESTAL}$. Here, the selection of the signal-related subspace dimension of the $\mathbf{V}_B$ matrix equals the number of frequency bins within the passing-band of interest. Then, for each grid point, the real and imaginary source images from the two perpendicular orientations (i.e., $\boldsymbol{\theta}$ and $\boldsymbol{\phi}$) were combined to create source-power images for each frequency bin for that epoch. Next, this procedure was repeated for all epochs in the 5-minute eyes-closed resting-state data. A set of 11 mean-source-power images (one for each low-frequency bin) was obtained by averaging source-power images across all epochs. The yellow and red "hot spots" highlighted by white arrows in Fig. 1(f) show an example of the frequency-domain VESTAL slow-wave source-power image from one subject at one specific frequency bin.

Regional slow-wave power diagram and normative database

Although the grid-point based frequency-domain VESTAL low-frequency source images have the advantage of high spatial resolution, it is difficult to use them directly for diagnosis. This is because the source images with thousands of grid-points introduce serious family-wise error associated with the multiple comparisons. In the present study, for each low-frequency bin, we created a region-based MEG slow-wave diagram by applying the cortical mask to the grid-point based frequency-domain VESTAL result. Essentially, this approach computed the total power for one of the 96 cortical regions defined in the mask by summing up the slow-wave power from all grid points within each region (Fig. 1(f)). This step generated a 96 (regions) by 11 (frequency-bin) diagram for each 5-minute eyes-closed data set as shown in Fig. 1(g).

One of the most important steps for using MEG low-frequency source imaging to detect abnormalities in TBI patients is the construction of a *normative database*. Fig. 1(g) illustrates the procedure of developing a normative database based on the region-based slow-wave power diagrams containing 96 cortical gray-matter regions and 11 low-frequency bins. In each subject, the three slow-wave power diagrams associated with three 5-minute eyes-closed data sets were first averaged to form one slow-wave power diagram per subject. Then, two 96×11 (cortical region by frequency) power-frequency matrices for the low-frequency range were obtained in the normative database — one contains the mean values by averaging across all 44 regional power-frequency diagrams and the second one contains the standard deviations (SD). Although the source-grid of the frequency-domain VESTAL contains an additional 15 sub-cortical gray-matter areas and the cerebellum, the present study only focuses on the 96 cortical gray-matter areas due to the lack of animal-based electrophysiological studies regarding pathological slow-waves in those sub-cortical gray-matter and cerebellar areas.

Finally, any region-based power-frequency diagram in the low-frequency range from a testing subject can be converted into a Z-

Table 1
Harvard–Oxford cortical gray-matter region labels and Percent likelihood of abnormal slow-wave generation for each cortical region. The integers in bold are the indices of the 96 cortical regions (L/R). Regions 1–48 are in left hemisphere; Regions 49–96 are in the right hemisphere. The three pairs of numbers are the Percent likelihood (%) of abnormal slow-wave generation from mild blast-induced, mild non-blast, and moderate TBI groups (L/R), respectively.

1/49: frontal pole			**13/61**: middle temporal gyrus temporooccipital part			**25/73**: frontal medial cortex			**37/85**: temporal fusiform cortex anterior division		
0.0/4.3	0.0/0.0	10.0/10.0	0.0/0.0	4.5/0.0	0.0/0.0	0.0/4.3	0.0/0.0	20.0/20.0	0.0/13.0	4.5/9.1	10.0/20.0
2/50: insular cortex			**14/62**: inferior temporal gyrus anterior division			**26/74**: juxtapositional lobule cortex SMA			**38/86**: temporal fusiform cortex posterior division		
0.0/0.0	0.0/0.0	10.0/0.0	0.0/4.3	0.0/0.0	0.0/10.0	0.0/0.0	9.1/9.1	0.0/10.0	0.0/4.3	9.1/4.5	0.0/20.0
3/51: superior frontal gyrus			**15/63**: inferior temporal gyrus posterior division			**27/75**: subcallosal cortex			**39/87**: temporal occipital fusiform cortex		
0.0/0.0	0.0/0.0	0.0/0.0	4.3/4.3	9.1/0.0	10.0/0.0	0.0/0.0	0.0/4.5	10.0/10.0	8.7/13.0	22.7/13.6	0.0/30.0
4/52: middle frontal gyrus			**16/64**: inferior temporal gyrus temporooccipital part			**28/76**: paracingulate gyrus			**40/88**: occipital fusiform gyrus		
0.0/4.3	4.5/0.0	0.0/10.0	0.0/0.0	9.1/0.0	10.0/10.0	13.0/4.3	9.1/18.2	0.0/10.0	8.7/8.7	9.1/18.2	0.0/0.0
5/53: inferior frontal gyrus pars triangularis			**17/65**: postcentral gyrus			**29/77**: cingulate gyrus anterior division			**41/89**: frontal operculum cortex		
0.0/4.3	4.5/9.1	10.0/0.0	4.3/4.3	0.0/0.0	0.0/10.0	4.3/17.4	18.2/9.1	10.0/0.0	4.3/17.4	0.0/18.2	10.0/0.0
6/54: inferior frontal gyrus pars opercularis			**18/66**: superior parietal lobule			**30/78**: cingulate gyrus posterior division			**42/90**: central opercular cortex		
0.0/0.0	4.5/9.1	10.0/10.0	0.0/0.0	4.5/0.0	10.0/10.0	4.3/4.3	13.6/9.1	0.0/0.0	4.3/4.3	4.5/13.6	0.0/10.0
7/55: precentral gyrus			**19/67**: supramarginal gyrus anterior division			**31/79**: precuneous cortex			**43/91**: parietal operculum cortex		
0.0/4.3	0.0/0.0	0.0/0.0	0.0/8.7	0.0/4.5	0.0/10.0	13.0/13.0	22.7/18.2	10.0/0.0	4.3/4.3	4.5/9.1	0.0/10.0
8/56: temporal pole			**20/68**: supramarginal gyrus posterior division			**32/80**: cuneal cortex			**44/92**: planum polare		
0.0/8.7	0.0/0.0	20.0/10.0	0.0/0.0	4.5/0.0	10.0/10.0	0.0/4.3	13.6/18.2	0.0/0.0	8.7/13.0	22.7/4.5	10.0/10.0
9/57: superior temporal gyrus anterior division			**21/69**: angular gyrus			**33/81**: frontal orbital cortex			**45/93**: Heschls gyrus H1 H2		
0.0/0.0	18.2/9.1	20.0/0.0	0.0/0.0	4.5/0.0	10.0/10.0	4.3/0.0	0.0/0.0	10.0/20.0	8.7/26.7	18.2/18.2	0.0/20.0
10/58: superior temporal gyrus posterior division			**22/70**: lateral occipital cortex superior division			**34/82**: parahippocampal gyrus anterior division			**46/94**: planum temporale		
0.0/4.3	4.5/0.0	0.0/0.0	0.0/0.0	0.0/4.5	0.0/10.0	0.0/4.3	9.1/4.5	10.0/20.0	13.0/0.0	13.6/0.0	10.0/0.0
11/59: middle temporal gyrus anterior division			**23/71**: lateral occipital cortex inferior division			**35/83**: parahippocampal gyrus posterior division			**47/95**: supracalcarine cortex		
0.0/8.7	4.5/13.6	20.0/10.0	0.0/0.0	9.1/4.5	0.0/0.0	4.3/13.0	18.2/13.6	20.0/30.0	34.8/21.7	22.7/22.7	20.0/20.0
12/60: middle temporal gyrus posterior division			**24/72**: intracalcarine cortex			**36/84**: lingual gyrus			**48/96**: occipital pole		
0.0/8.7	4.5/0.0	0.0/0.0	0.0/0.0	27.2/13.6	0.0/0.0	21.7/0.0	18.2/4.5	10.0/0.0	0.0/0.0	0.0/4.5	0.0/10.0

score diagram (96×11) as shown in Fig. 1(h) for a mTBI patient. Each element of this Z-score diagram is calculated by:

$$Z_{ij} = \left(P_{ij} - Mean_{ij}^{\ ctrl}\right)/SD_{ij}^{\ ctrl}, i = 1,2,\ldots,96, j = 1,2,\ldots,11 \quad (7)$$

where $Mean_{ij}^{ctrl}$ and SD_{ij}^{ctrl} are the mean and standard deviation values from the two 96×11 normative database matrices in healthy control subjects, containing the region-based power-frequency diagrams for the low-frequency range.

Detecting abnormal MEG slow-waves in TBI patients

One main goal of the present study is to use MEG low-frequency source imaging to assist with the diagnosis of individual TBI patients. To achieve this goal, we need to identify a MEG slow-wave variable (measure) that shows minimum overlap between healthy controls and TBI patients. We hypothesize that in a TBI patient, at least one region will generate statistically abnormal slow-wave, regardless of the exact location of that region. The previous adoption of the region-based MEG power-frequency diagram reduced the family-wise error due to multiple comparisons from thousands of grid points to 96 cortical gray-matter regions.

In this study, we use maximum Z-value of slow-wave measurement to detect brain areas with abnormal MEG slow-waves in TBI patients. In this approach, the Z-score diagrams (Eq. (7)) from the data sets in all healthy control subjects were calculated. Then, for each Z-score diagram, the maximum Z-value across 96 cortical regions and 11 frequency-bins was identified. Next, the maximum Z-value (i.e., Z_{max}) among three Z-score diagrams associated with three 5-minute eyes-closed resting-state datasets was obtained for each healthy control and TBI subject. The mean Z-value will not work effectively, due to the highly heterogeneous nature of the TBI. Unlike many other patient populations (e.g., schizophrenia) the brain areas injured by TBI are highly variable across individuals, and often without global effect. The MEG slow-wave generation characteristics in a TBI patient with right frontal lobe injury are quite different from those in another TBI patient with left temporal lobe injuries. Using the Z_{max} value (across cortical regions and frequency-bins) is equivalent to examining the hypothesis that at least one of the 96 cortical regions shows abnormal slow-waves.

Results

Determine the threshold for abnormal slow-wave power

Prior to applying the MEG slow-wave source imaging technique to TBI patients, we first determined the threshold of abnormal slow-wave power using the normative database. The problem of multiple comparisons needs to be addressed for 96 cortical regions and 11 frequency bind. In this approach, we adopted the standard Bonferroni correction threshold of 4.28 for Z-score associated with $p = 0.01$ after correcting for the 1056 (96×11) multiple comparisons. This threshold can be used to identify individual TBI patients with abnormally high MEG slow-wave power on a statistical basis.

Positive-finding rates of MEG frequency-domain VESTAL slow-wave exam for different groups of TBI patients

This sub-section provides one of the main findings of the present study. Fig. 2 shows the Z_{max} values, obtained from frequency-domain VESTAL low-frequency source imaging, plotted separately

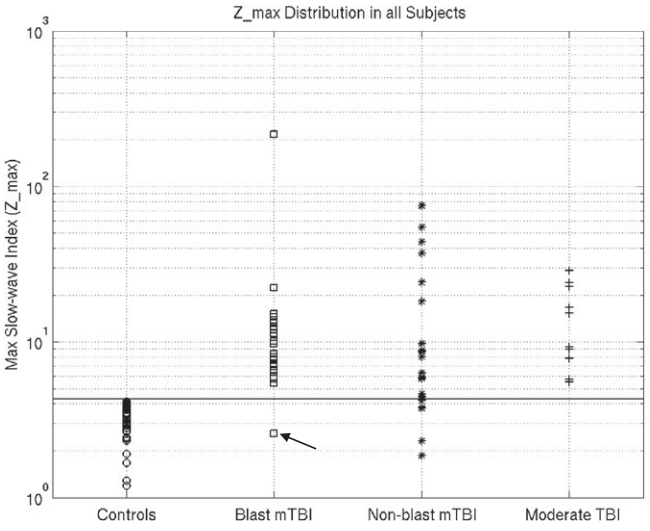

Fig. 2. Zmax values obtained from frequency-domain VESTAL low-frequency source imaging are plotted separately for 1) healthy control, 2) mild blast-induced TBI, 3) mild non-blast-induced TBI, and 4) moderate TBI groups. The y-axis is in logarithm scale. Zmax values from all healthy control subjects are below the solid horizon line indicating the threshold of 4.28 for p = 0.01 with Bonferroni correction. The arrow points to a blast-induced TBI patient with potential malingering as neuropsychological exams suggested.

for 1) healthy control, 2) mild blast-induced TBI, 3) mild non-blast-induced TBI, and 4) moderate TBI groups. The y-axis is in logarithmic scale because some TBI patients showed markedly high slow-wave powers which translated into markedly high Z_{max} values. The most striking finding is the low overlap of the Z_{max} values between each TBI group and the healthy control group, with the patients in all TBI groups showing markedly higher slow-wave Z_{max} values than the healthy control subjects. This property provides the basis of using our automated MEG low-frequency source imaging, based on frequency-domain VESTAL, for the diagnosis of TBI; and corroborates the well-known fact in the EEG literature, that focal delta-waves are not a normal finding in alert, awake adults, and that their presence signifies the presence of structural brain injury (Fisch, 1999; Rowan and Tolunsky, 2003).

With the 4.28 Z_{max} threshold, the positive finding rates were 96% for mild blast-induced TBI patients (22 out of 23), 77% for the mild non-blast TBI patients (17 out of 22), and 100% for the moderate TBI patients (10 out of 10). When we combined the blast-induced and non-blast mTBI groups together, the correct diagnostic rate was about 87% for the combined mTBI group. In contrast, the rates of positive findings using the conventional neuroimaging method (i.e., MRI clinical sequence listed previously, done at approximately the same time as the MEG) were 8.7%, 9.1%, 20.0%, and 8.9% for the same mild blast-induced TBI, mild non-blast TBI, moderate TBI, and combined mTBI (blast-induced plus non-blast) groups, respectively.

With positive-finding rates of the automated MEG low-frequency source imaging approach at such high levels, the difference between each TBI group and the healthy control group is expected to be highly significant (but not necessarily among different TBI groups). For completeness, we performed such ANOVA analyses, and the results confirm that in comparison to the healthy control group, the logarithm of Z_{max} values are indeed significantly higher in the mild blast-induced TBI ($F = 71.34$, $p < 10^{-11}$, $df = 65$), mild non-blast TBI ($F = 40.0$, $p < 10^{-7}$, $df = 64$), and moderate TBI ($F = 97.4$, $p < 10^{-12}$, $df = 52$) groups. However, there were no significant differences in the logarithm of Z_{max} values between the different TBI groups.

We also examine the test–retest reliability by using each of the three 5-minute sessions (instead of using the averaged value across the three sessions shown previously) from the 44 healthy control subjects to construct three different normative databases, for the first, second, and third 5-minute sessions, respectively. These three normative databases were then used to detect abnormal MEG slow-wave generations in patients from the three TBI groups. The positive finding rates in mild blast-induced, mild non-blast, and moderate TBI patients remained the same as the ones using the average values across three sessions, when using each of the three 5-minute sessions to construct the normative databases, but with one exception: the positive MEG slow-wave finding rate in mild non-blast TBI group became 82% (instead of 77%) when using the first 5-minute session in healthy control subjects to construct the normative database. This result suggests high across-session consistency in healthy control subjects.

One interesting case is a subject in the mild blast-induced TBI group who had a markedly lower Z_{max} value than the rest of the patients in that group, and similar to healthy control subjects, as indicated by the arrow in Fig. 2. Interestingly, this TBI subject also performed poorly on a Greens Word Memory Test (GWMT). GWMT was designed to measure effort, to identify and treat separately any data that are of doubtful validity owing to poor effort, whether in the assessment of single cases or in group research (Green, 2005). A clear pass is one in which the Immediate Recall and Delayed Recall are above 90%; a clear fail is one in which any one of these scores is at or below 82.5%; a caution appears if they are in between 83 and 90%. If any of these two primary test scores are at 82.5% score or below, there is a high probability that other test scores from the same person significantly underestimate the person's actual abilities owing to poor effort. This particular subject scored 70.0% for the Immediate Recall and 77.5% for Delayed Recall, definitely indicating poor effort. This example shows the consistency between MEG low-frequency source imaging and a neuropsychological test of poor effort or potential malingering.

Characteristics of injuries: blast-induced versus non-blast TBI, similarity and differences

Although the analysis using Z_{max} provides crucial diagnostic information, it does not address the loci and characteristics of abnormal slow-wave generation in TBI patients. In this section, we went beyond Z_{max} and examined individual cortical regions with slow-wave Z-scores above the 4.28 threshold in individual TBI patients. Fig. 3 shows the empirical (Kaplan–Meier) cumulative distribution function (ECDF) of Z-value of the data sets from all healthy control subjects (solid lines) and from all three groups of TBI patients combined (dashed lines), for 4 representative brain areas and each at one of the 11 low-frequency bins. In each of these 4 examples, the ECDF of TBI patients shows a shift towards the direction of high Z value indicating increased MEG slow-wave signal, compared with the healthy controls. The vertical lines indicate $Z = 4.28$, the abnormal slow-wave threshold for corrected p-value of 0.01. For these 4 areas, the numbers of data sets in TBI subjects that show MEG slow-waves beyond thresholds are 3, 1, 1, and 0, respectively. No data sets from healthy control subjects reach the thresholds.

Using the above method, we can identify the brain regions in each TBI patient that generate abnormal MEG slow-waves. Fig. 4 shows the three diagrams of cortical gray-matter areas (y-axis) that generate abnormal MEG slow-waves in individual patients (x-axis) from the mild blast-induced TBI (Fig. 4(a)), mild non-blast TBI (Fig. 4(b)), and moderate TBI (Fig. 4(c)) groups. For each subject (each column in a diagram), the black bars indicate the abnormal slow-wave generations that are above the threshold. The majority of patients showed at least one, and often many cortical gray-matter areas that generated significant slow-waves.

Each diagram in Fig. 4 can be analyzed in two different ways: i.e., across subjects and across different gray-matter regions. First, in across-subject group analysis, the numbers of cortical gray-matter

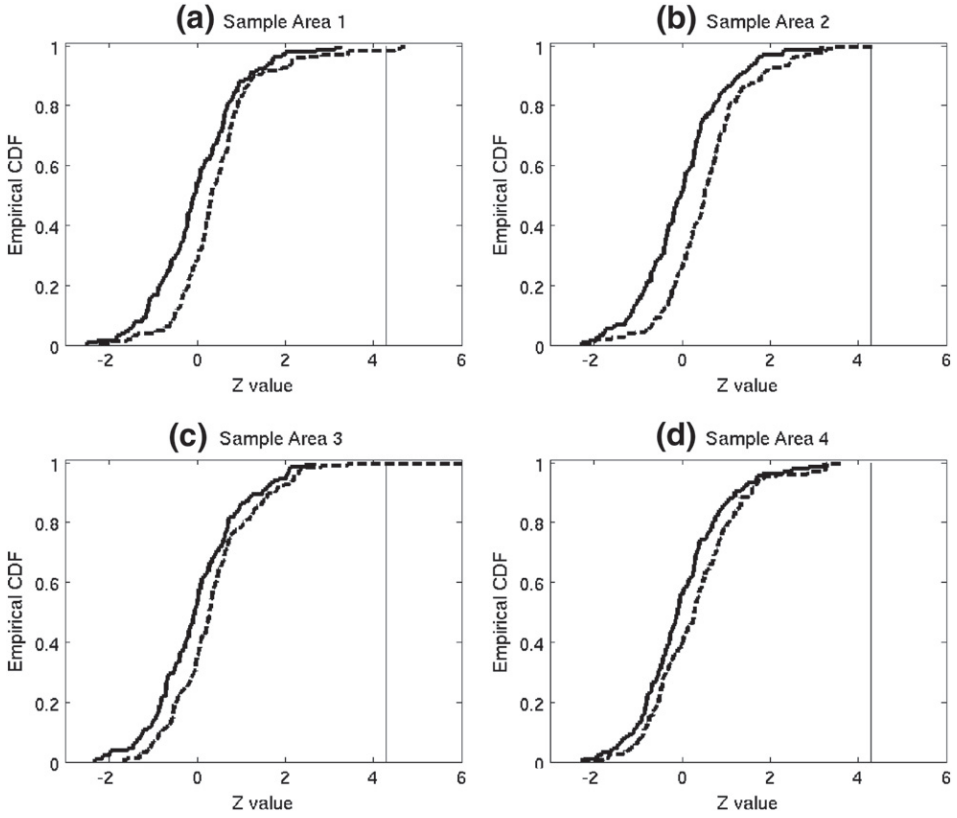

Fig. 3. Empirical (Kaplan–Meier) cumulative distribution function (ECDF) of Z-value of the data sets from all healthy control subjects (solid lines) and from all three groups of TBI patients combined (dashed lines), for 4 representative brain areas and each at one of the 11 low-frequency bins. The vertical lines indicate Z = 4.28, the abnormal slow-wave threshold for corrected p-value of 0.01.

regions that showed abnormal slow-waves were 4.3 ± 4.1, 7.0 ± 9.1, and 7.0 ± 8.5 for mild blast-induced, mild non-blast, and moderate TBI patients, respectively. No significant group differences were found for the number of gray-matter regions with abnormal slow-waves, due to the large variances. The fact that many cortical gray-matter regions showed abnormal MEG slow-waves reveals the diffuse nature of brain injuries in all three TBI groups, potentially due to TAI. No significant hemispheric asymmetry was found for the number of gray-matter regions with abnormal slow-waves in any of the TBI groups. There were 1 mild blast-induced TBI (i.e. the possible malingering subject described above); 5 mild non-blast TBI; and 0 moderate TBI patients that did not show any black bars, which indicates the low false negatives of the MEG low-frequency source imaging approach.

Next, with these three diagrams, we can further analyze the data across 96 different gray-matter regions (regions 1–48 in the left hemisphere, and analogous regions 49–96 in the right; see Table 1), and estimate the characteristics of neuronal injuries by calculating the likelihood of slow-wave generation in each cortical gray-matter region within each TBI group: for each row of these diagrams, by summing up across all columns and then dividing the result by the number of patients in each group, we obtained the percent likelihood of abnormal slow-wave generation for each cortical gray-matter region. Specifically, in each ROI, we calculated the percent likelihood of abnormal slow-wave generation in different TBI groups, which results in three sets of 96% likelihood values for the three TBI groups. Then, the statistical analyses were performed among these sets of

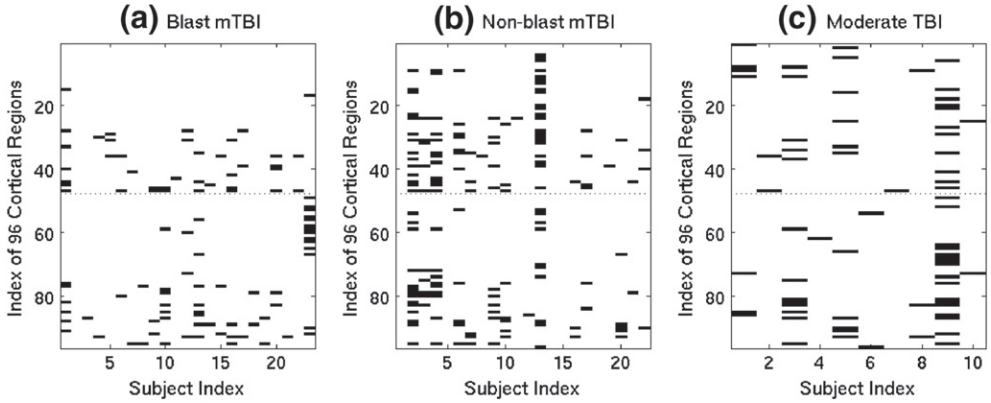

Fig. 4. Diagrams showing cortical gray-matter areas (y-axis) that generate abnormal MEG slow-waves in individual patients (x-axis) from the mild blast-induced (a), mild non-blast (b), and moderate (c) TBI groups. For each subject (each column in a diagram), the black bars indicate the abnormal slow-wave generations that are beyond the threshold. In each plot, the regions in the left hemisphere (regions 1–48) are separated from the ones in the right hemisphere (regions 49–96) by the dotted line.

percent likelihood values. The result is shown in Fig. 5(a) in which the color scale indicates the percent of likelihood for 96 cortical gray-matter regions for the three TBI groups. One interesting feature is the similarity of the characteristic between the mild blast-induced TBI (left column) and the mild non-blast TBI (middle column). This became more obvious when we plotted only these two groups in Fig. 5(b). Statistical analysis shows that the percent-likelihood of slow-wave generation as measured by count of abnormal Z scores of the mild blast-induced TBI group is highly and positively correlated with that of the mild non-blast TBI group ($r=0.55$, $p<10^{-8}$, $df=94$), as indicated by the asterisks and double-headed arrow in Fig. 5(a). Significant correlations were also found between the mild blast-induced TBI and moderate TBI groups ($r=0.26$, $p<.01$, $df=94$), but not between mild non-blast TBI and moderate TBI groups ($r=0.12$, $p=0.24$, $df=94$).

Despite the highly significant correlation between the characteristics of slow-wave generation between mild blast-induced TBI and mild non-blast TBI groups, there are also differences between these two groups. Fig. 5(c) shows the difference of percent likelihood measure between mild blast-induced versus mild non-blast TBI groups (i.e., the first column minus the second column in Fig. 5(a) or equivalently, the blue line minus the green line in Fig. 5(b)). A *t*-test was performed to assess such a difference in the percent likelihood of abnormal slow-wave generation across 96 ROIs in different mTBI groups. The result showed that the percent-likelihood of slow-wave generation in the non-blast mTBI group was significantly higher than that in the blast-induced mTBI group ($t=2.7$, $p<.01$, $df=95$).

The percent-likelihood values of abnormal MEG slow-wave generation for the three TBI groups are listed in Table 1. In the mild blast-induced TBI group, the left Supracalcarine cortex (cortical region #47 in Figs. 5(a) and (b) and Table 1) showed a high likelihood (34.8%) of generating abnormal slow-waves. The same region also shows relative high likelihood of abnormal MEG slow-wave generation in mild non-blast (22.7%) and moderate (20%) TBI groups. In the mild non-blast TBI group, left Intra-calcarine cortex (cortical region #24) showed a high likelihood of abnormal slow-wave generation (27.3%). In the moderate TBI group, the right Parahippocampal Gyrus posterior division (cortical region #83) and Temporal Occipital Fusiform Cortex (cortical region #87) showed a high likelihood of abnormal slow-wave generation, both at 30%. The percent-likelihood values of abnormal MEG slow-wave generation are also shown in Fig. 6 as color-coded gray-matter areas in MNI-152 atlas space for the three TBI groups. The information in Fig. 6 and Table 1 is essentially the same, but with different formats of presentation.

Among the regions that showed abnormal slow-waves in all TBI patients (i.e., three TBI groups combined), in 46% of the cases abnormal slow-waves were found in all three 5-minute sessions, whereas in the remaining cases slow-waves were found in either one or two sessions. No particular 5-minute session showed statistically higher/lower chances of MEG slow-wave generation than the other two sessions.

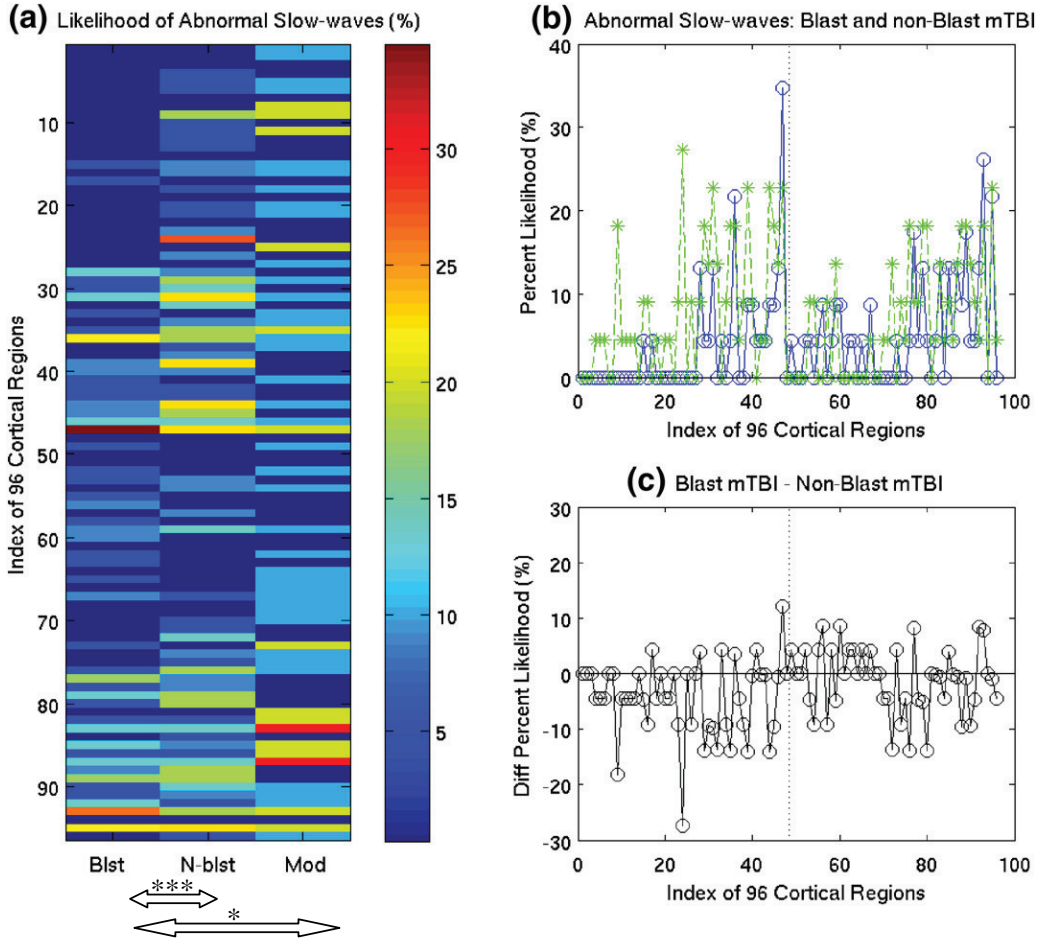

Fig. 5. (a) Percent likelihood of abnormal slow-wave generation for each cortical gray-matter region in three TBI groups. The two mTBI groups are highly correlated and the mild blast group was also correlated with the moderate non-blast group (double-headed arrows). (b) A different way to plot the percent likelihood of abnormal slow-wave generation for mild blast-induced (blue color) and mild non-blast (green color) TBI groups. (c) Difference of percent likelihood of abnormal slow-wave generation (blast-induced minus non-blast) showing the blast group having fewer regions that were affected by TBI than non-blast group. The vertical dotted lines in (b) and (c) divide the regions in the left hemisphere from the ones in the right hemisphere.

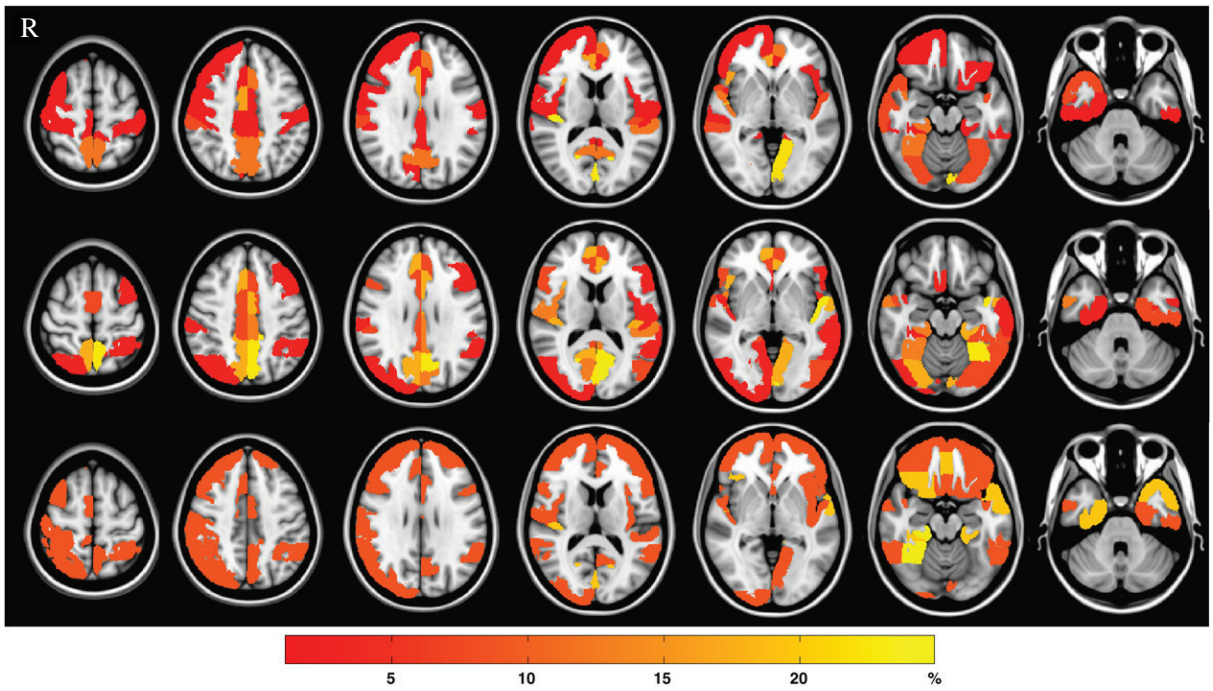

Fig. 6. Percent-likelihood of MEG abnormal slow-wave generation (in MNI-152 Atlas space) from mild blast-induced TBI (top row), mild non-blast TBI (middle row), and moderate TBI (bottom row) groups.

MEG low-frequency source imaging correlates with post-concussive symptoms

We also examined the relationship between abnormal MEG slow-waves and the 21 PCS from the modified HISC in all 55 TBI patients. The total PCS scores (summing up over all categories) were: 6.4 ± 1.5 for mild blast-induced TBI group, 6.5 ± 3.1 for the mild non-blast TBI group, and 5.3 ± 2.7 for the moderate TBI group. No significant group differences were observed among the three different TBI groups. None of the healthy control subjects reported any PCS.

To compute the correlation between MEG slow-wave and PCS, we first calculated the total number of brain regions that generated abnormal slow-waves in each TBI patient, called "$N_{slow\text{-}wave\_sum}$". Next, we calculated the total symptom score by summing up all 21 PCS categories in each TBI patient, called "N_{PCS_sum}". Then, we computed the correlation between $N_{slow\text{-}wave\_sum}$ and N_{PCS_sum} and found that these two were significantly and positively correlated ($r = 0.27$, $p < 0.05$, $df = 53$). Next, we performed exploratory correlation analyses between the total number of regions that generated MEG slow-waves and each of the 21 individual PCS categories in these TBI patients. Prior to the Bonferroni correction, the $N_{slow\text{-}wave\_sum}$ positively correlated with Apathy ($r = 0.36$, $p < 0.01$), Personality Changes (e.g., social problems) ($r = 0.32$, $p < 0.05$), and Blurred Vision and other visual difficulties ($r = 0.27$, $p < 0.05$). These correlations became not significant after the Bonferroni correction. We also performed a stepwise linear regression with MEG slow-wave ($N_{slow\text{-}wave\_sum}$) as the dependent variable and the 21 PCS symptoms as the independent variables. In doing so, there was a trend ($p = 0.07$) for Apathy to account for 13% of the $N_{slow\text{-}wave\_sum}$ variance.

We also examined the correlation between the Zmax values and PCS in all TBI patients. The result showed that the Zmax value positively correlated with the symptom of Affective Lability (quick-changing emotions) with $r = 0.62$, $df = 53$, uncorrected $p < 10^{-6}$, and $p < 10^{-4}$ after the Bonferroni correction. No other symptoms, or the total symptom score, showed significant correlations with the Zmax value.

In additional analyses, we did not find a significant difference between the eight TBI patients with multiple injuries and the remaining TBI patients in MEG slow-wave generation. As a sample size of eight is small, additional research is needed to determine if patients with multiple TBIs show some unique characteristics of brain functioning relative to patients with a single TBI. In addition, the count of abnormal Z scores did not significantly correlate with the time-since-injury. This was probably due to the heterogeneous nature of TBI. Longitudinal studies that assess the same TBI patients with multiple MEG exams are needed to address this topic.

Analyses of MEG slow-wave generations at different frequency bins

Analyses of abnormal MEG slow-wave generation at different frequency bins were conducted to examine: 1) whether specific frequency bins showed more/less MEG slow-waves than the others; 2) whether the slow-waves generations across different frequency bins correlated to each other; and 3) whether slow-wave generation at any frequency bin correlated with clinical symptoms. In these analyses, we first identified the frequency bins that showed abnormal slow-waves in each TBI patient, regardless of which cortical region(s) the slow-waves were from. This step created three 2D matrices (frequency bins by subject index) for the three TBI groups, with each element being "1" for "Yes", and "0" for "No" abnormal slow-waves. Figs. 7(a)–(c) show these matrices, with the black bars being the frequency bins that showed abnormal slow-waves. After the Bonferroni correction, no particular frequency bin showed significantly higher/lower chance of generating abnormal slow-wave than the other bins, in any of the TBI groups or when combining all three TBI groups together. However, we did find significant correlations in MEG slow-wave generation between different frequency bins when combining all TBI patients together (Fig. 7(d)). In this approach, we collocated the above three matrices and formed an 11 by 55 matrix (i.e., number of frequency bins by number of TBI patients), $H_{freq\_bin\_slow\_wave}$, and calculated the correlations between every pair of frequency bins (i.e., correlation for every pair of rows in this combined matrix). Only the significant correlations with corrected $p < .05$ (Bonferroni corrected) were shown. The main findings are: the slow-wave generations among Bins 1–4 were highly correlated; Bins 3 and 4 were both

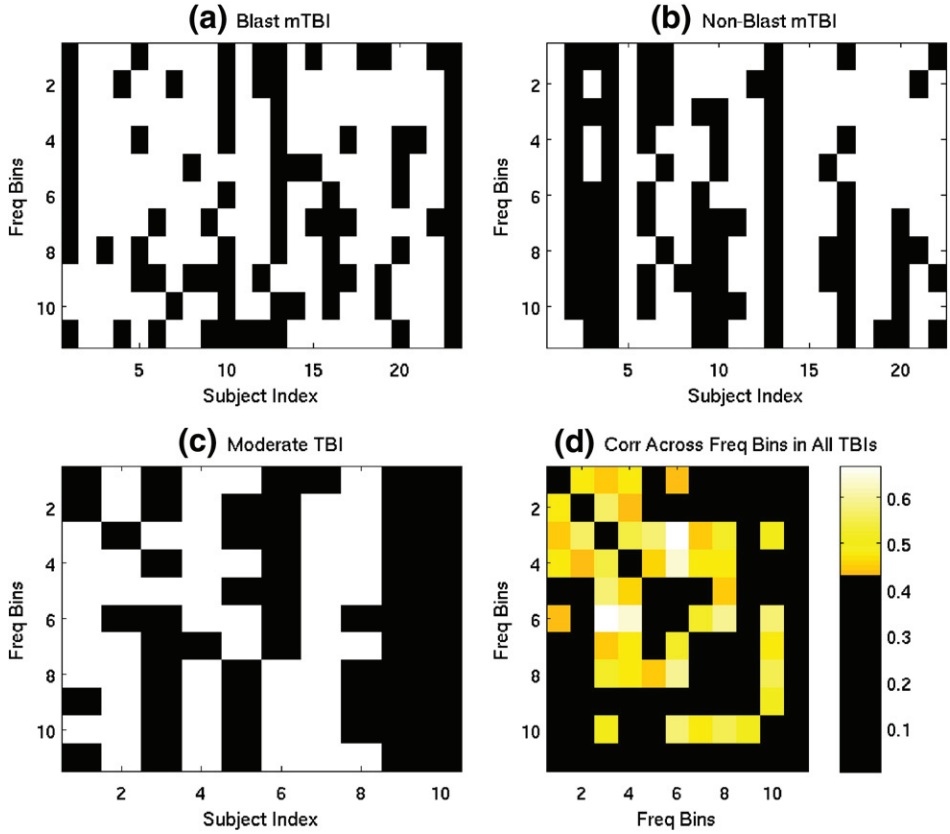

Fig. 7. Diagrams showing abnormal MEG slow-wave generation across different frequency bins (y-axis) in individual patients (x-axis) from the mild blast-induced (a), mild non-blast (b), and moderate (c) TBI groups. For each subject (each column in a diagram), the black bars indicate the abnormal slow-wave generations that are beyond the threshold. (d) Significant correlations in MEG slow-wave generation between different frequency bins when combining all TBI patients together. Only the significant correlations with corrected $p<.05$ (Bonferroni correction) were shown. The self-correlations in the diagonal were removed.

highly correlated with Bins 5–8; and Bin 10 was significantly correlated with Bins 3, and 6–9.

We examined the correlations between slow-wave generation at each frequency bin in $H_{freq\_bin\_slow\_wave}$ and the clinical symptoms in all 55 TBI patients. Prior to the Bonferroni correction, the results showed that: 1) slow-wave generation at Bin 3 (1.96 Hz) positively correlated with Apathy ($r=0.40$, $p<.01$) and Personality Changes (e.g., social problems) ($r=0.31$, $p<0.05$); 2) slow-wave generations at both Bin 2 (1.47 Hz) and Bin 5 (2.93 Hz) positively correlated with Difficulty with Speech ($r=0.37$, $p<.01$; $r=0.27$, $p<.05$, respectively); 3) slow-wave generations at both Bin 4 (2.44 Hz) and Bin 7 (3.91 Hz) positively correlated with the symptoms of Irritability, Lack of Patience, Easy Loss of Temper ($r=0.28$, $p<.05$; $r=0.30$, $p<.05$, respectively); and 4) however, only the correlation between slow-wave generation at Bin 3 and Apathy survived the Bonferroni correction. In addition, the slow-wave generation at Bin 3 was found to be positively correlated with the total symptom score N_{PCS_sum} ($r=0.35$, $p<0.01$).

Discussion

Using a novel and automated MEG low-frequency source imaging approach, we found abnormal delta-waves in 87% of 45 patients with mTBI (23 with blast and 22 with non-blast causes); and 100% of 10 patients with moderate TBI (Fig. 2). These positive-finding rates are markedly higher than the ~9% and 20% rates using the conventional neuroimaging approaches (i.e., MRI) in the same mild and moderate TBI patients, respectively. We are not aware of any other neuroimaging approaches that have achieved the same sensitivity as our MEG approach. At the threshold of 4.28 for the Z_{max} which is associated with $p=0.01$ after the Bonferroni correction, none of our 44 normal controls showed abnormal slow-waves. Our result is consistent with the general conclusion from an MEG study in mTBI by Lewine and colleagues (Lewine et al., 1999; Lewine et al., 2007), except the positive-finding rates in the present study were higher.

We believe that two reasons explain our high positive-finding rates from the new automated MEG low-frequency source imaging approach based on frequency-domain VESTAL. First, the diagnosis in our new approach is based on making an objective comparison with a control normative database containing MEG slow-wave source power from 96 cortical regions. The source imaging analysis is performed by analyzing all the artifact-free epochs from the entire resting-state recording. The procedure is objective since no human interaction is involved in manually selecting the epochs. Furthermore, our approach is based on imaging results of slow-waves in source space rather than sensor space. This is substantially different from the conventional approaches, in which an operator with experience selects the sensor-waveform epochs that he/she considers to demonstrate abnormal low-frequency MEG signals.

Second, the MEG low-frequency source imaging has the advanced features in frequency-domain VESTAL. It has been shown that the VESTAL approach can localize neuronal sources with a variety of spatial profiles such as focal, multi-focal, dipolar, as well as distributed sources, and a variety of temporal profiles with uncorrelated, partially-correlated, as well as 100% correlated source time-courses (Huang et al., 2006). It has also been shown that the generators of abnormal slow-waves in mTBI patients can be in one or more of the above spatial-and-temporal profiles (Huang et al., 2009), ideal for the VESTAL approach. In contrast, the conventional MEG slow-wave source analysis used single-dipole fit (Lewine et al., 1999, 2007) which limited its ability to analyze MEG signals with complicated

neuronal-source configurations, which may include some cases of abnormal slow-waves in TBI patients.

An additional advantage of our neuroimaging approach, shared with other MEG protocols which detect delta slow-waves, is that the resting-state MEG recording procedure is spontaneous, requiring almost no effort from TBI patients, and is thus independent of patients' performance and effort. With the wide availability of information about TBI symptomatology and commonly-used psychometric tests on the Internet, and the variety of motivations for patients to exaggerate/understate symptoms and deficits (legal, financial, as well as healthcare factors, etc.) more objective diagnostic tests such as this resting-state MEG exam, which cannot be easily manipulated/"gamed", are invaluable. Of course, the factors that may increase slow-wave power need to be controlled in the MEG exam, as we did in the present study. These factors are: neuroleptic, sedative, or hypnotic medications, sleep deprivation, as well as other neurological disorders (e.g., stroke, epilepsy, brain tumor, etc.).

The present study also revealed the diffuse nature of the neuronal injuries in TBI patients (Figs. 4, 5, and 6). On average, approximately 4–8 cortical gray-matter areas showed abnormal slow-wave generation in each TBI patient using our automated MEG low-frequency source imaging. Such findings are consistent with the mechanism of diffuse axonal injury in TBI due to a combination of linear and rotational acceleration and deceleration (Adams et al., 1989; Arfanakis et al., 2002; Basser, 1995; Huisman et al., 2004; Xu et al., 2007). The findings are also consistent with our previous MEG-DTI study in mTBI, in which we found that abnormal MEG slow-waves are generated from cortical gray-matter areas that connect to white-matter fibers with reduced DTI fractional anisotropy due to axonal injury in patients with mTBI. Specifically, the reduced DTI fractional anisotropy in local white-matter fiber tracts led to focal abnormal MEG slow-waves from neighboring gray matter in mTBI. On the other hand, reduced anisotropy in major white-matter fiber tracts led to multi-focal or distributed patterns of abnormal slow-waves generated from cortical gray-matter areas that can be remote in location, but functionally and structurally linked by the injured major/long white-matter fiber tracts (Huang et al., 2009). The diffuse nature of MEG slow-wave generation is also consistent with a recent DTI study in blast mTBI subjects which showed reduced FA in a diffuse, widespread, and spatially variable pattern (Davenport et al., 2012).

The diffuse nature of abnormal MEG slow-wave generation in TBI also raises questions about the conventional neuroimaging analysis of group-averaging of source locations in space. Unlike abnormal slow-wave generation in patient populations with specific psychiatric and neurological disorders such as schizophrenia (Canive et al., 1996, 1998; Fehr et al., 2001, 2003; Rockstroh et al., 2007) and Alzheimer's disease (Fernandez et al., 2002) where group-averaging of source locations in space yielded meaningful information about dysfunctional neuronal networks, the loci that showed abnormal slow-wave generations in TBI patients tend to be highly variable in location. Hence, group-averaging of MEG slow-wave source locations in space is unlikely to be the most effective way to detect brain injuries. Instead, analyses of the MEG slow-wave generation characteristics, such as that introduced in the present study, may provide more insights about the neuronal injuries in TBI.

The analyses in Figs. 5(a) and (b) show that the percent likelihood of abnormal MEG slow-wave generation measured by Z scores in the mild blast-induced TBI group is highly and positively correlated with that of the mild non-blast TBI group, which indicates common characteristics of injuries between these two mTBI populations. To our knowledge, this is the first time that highly similar abnormal slow-wave generation characteristics are reported between symptomatic blast-induced and non-blast TBI patients. Our result is consistent with recent research that compared the neuropsychological outcomes from 86 U.S. military service members with blast versus non-blast mTBI and found no significant group differences on any neurocognitive measures (all $p > .05$) with the exception of the CPT-II Commissions (Lange et al., in review). It was suggested that the mechanism of blast-related CNS injuries is similar to that of the other head injuries, e.g., (Cernak et al., 2001). As we mentioned previously, in active-duty military personnel and veterans with blast-induced mTBI, brain injuries due to "pure" blast wave are not as common as we expected. Tertiary injuries (due to fall, hitting other objects, being hit by other flying objects, etc.) are common in blast-induced TBI as tertiary injuries — 17 out of 23 or 74% of our blast-induced TBI patients had tertiary injuries. The nature of the tertiary injuries in blast-induced mTBI is similar to that in civilian non-blast mTBI patients. This can explain the highly significant correlation of MEG slow-wave generation characteristics between the mild blast-induced TBI and mild non-blast TBI groups in the present study. Animal research extensively reviewed by Leung et al. (2008) shows transmission of a pressure wave into the brain during the blast; neuronal injuries, microglial and astroglial cell activation were evident after exposure to overpressure. However, the injury mechanisms unique to blast "at both the macroscopic and molecular level are still undefined and injury criteria still remain to be determined" (Leung et al., 2008). It is interesting that the patients with mild blast-induced TBI who reported tertiary injuries also experienced LOC and PTA, which indicates that these patients can recall, to some extent, what happened prior to the LOC and PTA. This suggests that the LOC and PTA may not be caused solely by the initial blast. In addition, it is difficult to completely rule out the possibility of tertiary injury in TBI patients who cannot remember whether they have tertiary injury. The brain that was initially set into motion by the blast energy often must stop at the end by interacting with other objects. More research needs to be done to fully understand the combinatorial impacts of the initial blast and tertiary injuries.

Despite the high correlations of the slow-wave generation characteristics in mild blast-induced and mild non-blast TBI (i.e., the two curves go up-and-down in a similar fashion, see Figs. 5(a) and (b)), the percent-likelihood values in the mild non-blast TBI curve are significantly higher than the ones in the mild blast-induced TBI curve (Fig. 5(c)). This difference may result from the combat helmet and armor used by military personnel which provides some protection against the effects of blast. Besides the well-documented protective effect of a helmet to non-blast head injuries in sports (Levy et al., 2004), viscoelastic foam pads like those in advanced combat helmets (ACH) reduced blast impact to the brain (Moss et al., 2009) or slightly mitigate intracranial stresses (Nyein et al., 2010).

It was also interesting that the percent likelihood of abnormal MEG slow-wave generation across ROI correlated significantly between the mild blast and the moderate non-blast TBI groups, but not between mild non-blast and moderate non-blast TBI groups. Due to the smaller number of subjects in this group ($N = 10$), we hesitate to conclude that moderate TBI has different or similar characteristics of slow-wave generation than mTBI. Further research with more subjects is needed to address this issue.

One unexpected finding in the present study is that the number of cortical gray-matter regions that generate abnormal MEG slow-waves in moderate TBI patients does not statistically differ from those in the two mTBI patient groups. This result appears to be counter-intuitive since one would expect that the moderate TBI patients would show more regions generating abnormal MEG slow-waves. We believe one reason for this finding is probably due to the context in which the designation of moderate versus mild diagnosis was made, based on the *acute* assessments of the TBI, such as loss of consciousness, initial GCS, and post-traumatic amnesia. In contrast, the MEG exam was performed in the sub-acute or chronic phases. It is possible that the clinical symptoms in moderate TBI patients diminished to a level similar to those of symptomatic mTBI patients by the time of the MEG assessment. This explanation is supported by the result that the PCS assessment at the time of the MEG exam significantly correlated with the MEG slow-wave measurement, and furthermore by the

finding that no significant group differences were observed for the PCS among the three different TBI groups at the time of MEG exam (see last sub-section in the Results).

Another reason for this finding would be that the mTBI patients in our study were all symptomatic, with ongoing PCS at the time of MEG assessment. At 6–9 months post-incident, most of the mTBI patients are symptom-free, and ~10–30% of the patients still have on-going PCS (Alexander, 1995; Binder, 1986, 1997; Bohnen et al., 1992; Rimel et al., 1981; Rutherford, 1989). Since the average time of our MEG assessment was 8.2 months post-incident, it is possible that symptomatic mTBI patients no longer significantly differ in severity from moderate TBI patients who also have on-going PCS. It has been shown by Lewine et al. (1999) that the asymptomatic mTBI patients do not show as much abnormal MEG slow-waves as the symptomatic mTBI patients do. Hence, if one examines mild and moderate TBI patients acutely when all patients have symptoms, it is possible that the MEG slow-waves may differentiate moderate and mild TBI in terms of injury severity.

The times of the MEG exam for the TBI patients in the present study were from 4 weeks to 3 years (mean 8.2 ± 7.1 months) post-injury, including sub-acute and chronic TBI patients. The sensitivity (and specificity) of *some* neuroimaging techniques may optimally apply to either acute or chronic time-windows, but not both. For example, in patients with stroke, diffusion-weighted imaging (DWI) is sensitive to acute injuries but not sensitive to chronic injuries; whereas structural abnormalities may not be visible in the acute phase, but become evident in T2- and T1-weighted MRI in the chronic stage. Although the present study shows that MEG slow-wave imaging is potentially sensitive to neuronal injuries in *both* sub-acute and chronic phases in symptomatic TBI patients, longitudinal studies with repeated measures are needed to address this issue.

Although the 15 sub-cortical gray-matter areas and cerebellum were part of the source space (in addition to the 96 cortical regions) for VESTAL analysis, these sub-cortical areas were not used for differentiating TBI patients from healthy control subjects due to several concerns. First, it is debatable whether MEG is sensitive to signals from these sub-cortical areas, because the neuronal magnetic fields decrease as $\sim 1/r^2$ for magnetometors and $\sim 1/r^3$ for gradiometers. Moreover, the contributions to the measured MEG signal from deep sub-cortical gray-matter neurons are much less than that from cortical neurons. Second, unlike cortex in which cortical neurons form columns and neurons in each column have similar orientations good for signal summation, the orientations in sub-cortical gray-matter neurons are not organized in well defined columns and laminae, which lead to less signal summation. Lastly, there is a lack of electro-neurophysiological studies in animals about slow-wave generation from sub-cortical gray-matter neurons due to de-afferentation caused by axonal injuries.

Based on our EOC recordings, the eye-movement related artifacts were uncommon in the eyes-closed recording. The epochs with EOG signal above 150 μV (very rare) were removed from the analyses. The MaxFilter was helpful to remove small eye-movement activities. Furthermore, the residual eye-movement signals were removed using our customized version of ICALAB. Usually, eye-movement related low-frequency artifacts have a unique MEG field distribution in the anterior frontal lobe. We did not see such a field distribution in our subjects' MEG data.

With noise in the MEG measurements, not all the 306 MEG measurements are independent. Dimension reduction of the gain (lead-field) matrix is needed to deal with independent spatial modes. The MaxFilter reduced the independent special modes to 64, and it was shown that the signal loss was negligible with such a truncation, even for data with high SNR evoked MEG data (Taulu et al., 2004a). There are concerns about minor signal loss for sources with high spatial frequency, typically associated with high gamma band signal, but not with the low frequency bands (delta, theta, alpha, or beta) (personal communication with Taulu). The noise level in resting-state MEG data is higher than that in evoked data sets, so that we can select the truncation of 40 during the frequency domain VESTAL analysis without losing the ability to localize measurable MEG signal. The process of removing artifacts with ICA was to remove a few artifact-related temporal modes. This procedure was done for the MEG sensor wave-form matrix, and not the MEG lead-field (gain) matrix. This process will not reduce the independent spatial modes of the MEG gain (lead-field) matrix.

Our group classification for different TBI groups was solely based on *clinical* criteria, consistent with most other TBI studies. We realize that some researchers (especially in non-imaging TBI studies) change their TBI classifications based on additional imaging findings (typically acute imaging findings). Although two mild blast-induced TBI and two non-blast TBI patients showed some "positive" findings on our chronic MRI exams, we did not re-classify them into the moderate category, because the classification is based only on clinical criteria. Furthermore, as mentioned in the section on Research Subjects, the "positive" MRI findings on the chronic MRI scans were nonspecific mild white-matter T2-prolongation, which may not have been related to head trauma; and none of the patients had intracranial hemorrhage or hemosiderin.

There are several limitations of the present study that warrant consideration. 1) The number of subjects in the moderate TBI group is smaller than the other two mTBI groups, which limited our ability to assess the common and different characteristics of injuries between moderate and mTBI patients. 2) Our clinical TBI PCS score only assesses the presence or absence of individual symptoms. We are in the process of implementing different scoring systems for PCS, which would provide a measure of symptom severity. 3) It is important to recognize that abnormal slow-wave activity is not pathognomonic to TBI. Instead, abnormal delta-waves may be present in other neurological or psychiatric disorders such as stroke infarct, epilepsy, brain tumor, Alzheimer disease, or schizophrenia. However, in clinical practice, these disorders can be easily excluded based on structural MRI and medical history. We screened the subjects carefully and excluded those with the above disorders from entering the present study. 4) Certain medications (e.g., some sedative neuroleptics and hypnotics) are known to increase delta-wave power (Niedermeyer and Da, 2005). This was not a confounding factor in our study as patients taking these medications were either excluded from participation or stopped taking them for three half-lives prior to the MEG exam. 5) Many subjects did not have "pure" blast mTBI in our blast-induced group since they reported tertiary head injuries. Although it is preferable to study pure samples of blast mTBI, these subjects were difficult to find in our active-duty military population and may not represent the typical blast-induced TBI patient population. All research in this field must balance the purity of the sample with the representativeness and availability of subjects in the active-duty military population. 6) We excluded subjects with diagnosed psychiatric disorders including PTSD. It can be challenging to make a differential diagnosis between mTBI and PTSD due to an overlap in clinical symptoms and cognitive deficits. Many active-duty military personnel and VA patients have co-morbid mTBI and PTSD. Presently, there is not sufficient evidence to suggest that PTSD patients without mTBI show abnormal MEG slow-waves, but we cannot completely rule out the PTSD factor in our blast-induced TBI sample. 7) It is a concern if the findings of abnormal slow-waves in TBI patients are unique to the eyes-closed condition or if they can also be found in eyes-open condition. A similar concern is if sleepiness may affect the TBI-related MEG slow-waves. We took measures to minimize potential differential effects of sleepiness in our subjects by alternating between eyes-open and eyes-closed sessions. Still, the eyes-open MEG data were contaminated with eye-blink artifacts. Until we can effectively remove the eye-blink artifacts, we cannot address this concern. 8) We did not directly assess the false-positive rate in the present

study. Although none of our 44 healthy control subjects showed positive MEG slow-wave findings beyond the $p = .01$ ($Z_{max} = 4.28$) threshold, we cannot claim that the false-positive rate is zero since the same 44 controls were used to construct the normative database. The appropriate way to assess the false-positive rate will be to recruit additional healthy controls with similar size (e.g., ~44), which we plan to do in future studies. 9) It has been suggested in some on-going studies that recruitment of deployed, but not injured active-duty personnel as healthy control subjects is preferred for studying blast-induced TBI (http://clinicaltrials.gov/ct2/show/NCT00754169). However, the primary purpose of this study was to compare blast-induced injury with injury from other causes. Since subjects with non-blast injuries were drawn primarily from the civilian population, a mixed control group would be ideal. In practice, recruiting deployed, but not injured active-duty personnel as healthy control subjects has been challenging due to concerns that participation in research would impact the tight training schedule of these individuals. In future studies, inclusion of both military and civilian control subjects will be a high priority.

In summary, the present study examined the sensitivity of our new automated and operator-independent MEG low-frequency (slow-wave) source imaging method in mTBI (with blast and non-blast causes) and moderate TBI. The results show that this new MEG low-frequency source imaging method achieves a positive-finding rate of 87% for the mTBI group (blast-induced plus non-blast) and 100% for the moderate group, with the threshold chosen at $p < .01$ level. The result also shows that the characteristics of slow-wave generation in mild blast-induced TBI and mild non-blast TBI patients are significantly correlated. Furthermore, among 96 cortical regions, the likelihood of abnormal slow-wave generation was less in mild blast-induced TBI patients than in mild non-blast TBI patients, suggesting possible protective effects; it may be due to military helmets and armor, or the mechanism of injury. Finally, the results show significant correlations between the number of cortical regions that generate abnormal slow-waves and the total post-concussive symptom scores in TBI patients. The present study provides a foundation for the use of MEG low-frequency (slow-wave) source imaging for assisting with the clinical diagnosis of TBI. As we move forward in better understanding the utility of the MEG in assessing the TBI population we would like to better understand how individual symptoms and their severity contribute to positive MEG findings and the clinical picture.

Acknowledgments

This work was supported in part by Merit Review Grants from the Department of Veterans Affairs (two for M.X. Huang, one R.R. Lee), National Football League (M.X. Huang and R.R. Lee), and McDonnell Foundation via the Brain Trauma Foundation (PI: J. Ghajar, site PIs: R.R. Lee and M.X. Huang). We would like to thank Angelica Dilay, Susan Yoder, Richard Daugherty, and Terry Curry (RN) for their efforts in recruiting TBI patients, and Dr. J. Chris Edgar for helpful suggestions to the manuscript. We would also like to thank the anonymous reviewers' constructive suggestions that substantially strengthen the present study.

Disclaimer: the views expressed in this article are those of the authors and do not necessarily reflect the official policy or position of the Department of the Navy, Department of Defense, or the U.S. Government.

References

Adams, J.H., Doyle, D., Ford, I., Gennarelli, T.A., Graham, D.I., McLellan, D.R., 1989. Diffuse axonal injury in head injury: definition, diagnosis and grading. Histopathology 15, 49–59.

Alexander, M.P., 1995. Mild traumatic brain injury: pathophysiology, natural history, and clinical management. Neurology 45, 1253–1260.

Arfanakis, K., Haughton, V.M., Carew, J.D., Rogers, B.P., Dempsey, R.J., Meyerand, M.E., 2002. Diffusion tensor MR imaging in diffuse axonal injury. AJNR Am. J. Neuroradiol. 23, 794–802.

Baayen, J.C., de, J.A., Stam, C.J., De Munck, J.C., Jonkman, J.J., Trenite, D.G., Berendse, H.W., van Walsum, A.M., Heimans, J.J., Puligheddu, M., Castelijns, J.A., Vandertop, W.P., 2003. Localization of slow wave activity in patients with tumor-associated epilepsy. Brain Topogr. 16, 85–93.

Ball, G.J., Gloor, P., Schaul, N., 1977. The cortical electromicrophysiology of pathological delta waves in the electroencephalogram of cats. Electroencephalogr. Clin. Neurophysiol. 43, 346–361.

Basser, P.J., 1995. Inferring microstructural features and the physiological state of tissues from diffusion-weighted images. NMR Biomed. 8, 333–344.

Basser, P.J., Pierpaoli, C., 1996. Microstructural and physiological features of tissues elucidated by quantitative-diffusion-tensor MRI. J. Magn. Reson. B 111, 209–219.

Bazarian, J.J., Zhong, J., Blyth, B., Zhu, T., Kavcic, V., Peterson, D., 2007. Diffusion tensor imaging detects clinically important axonal damage after mild traumatic brain injury: a pilot study. J. Neurotrauma 24, 1447–1459.

Benson, R.R., Meda, S.A., Vasudevan, S., Kou, Z., Govindarajan, K.A., Hanks, R.A., Millis, S.R., Makki, M., Latif, Z., Coplin, W., Meythaler, J., Haacke, E.M., 2007. Global white matter analysis of diffusion tensor images is predictive of injury severity in traumatic brain injury. J. Neurotrauma 24, 446–459.

Bigler, E.D., Orrison, W.W., 2004. Neuroimaging in sports-related brain injury. In: Lovell, M.R., Echemendia, R.J., Barth, J.T., Collins, M.W. (Eds.), Traumatic Brain Injury in Sports: An International Perspective. Swets and Zeitlinger, Lisse, Netherlands, pp. 71–94.

Binder, L.M., 1986. Persisting symptoms after mild head injury: a review of the post-concussive syndrome. J. Clin. Exp. Neuropsychol. 8, 323–346.

Binder, L.M., 1997. A review of mild head trauma. Part II: clinical implications. J. Clin. Exp. Neuropsychol. 19, 432–457.

Bohnen, N., Jolles, J., Twijnstra, A., 1992. Neuropsychological deficits in patients with persistent symptoms six months after mild head injury. Neurosurgery 30, 692–695.

Brang, D., Hubbard, E.M., Coulson, S., Huang, M., Ramachandran, V.S., 2010. Magnetoencephalography reveals early activation of V4 in grapheme-color synesthesia. Neuroimage 53, 268–274.

Canive, J.M., Lewine, J.D., Edgar, J.C., Davis, J.T., Miller, G.A., Torres, F., Tuason, V.B., 1998. Spontaneous brain magnetic activity in schizophrenia patients treated with aripiprazole. Psychopharmacol. Bull. 34, 101–105.

Canive, J.M., Lewine, J.D., Edgar, J.C., Davis, J.T., Torres, F., Roberts, B., Graeber, D., Orrison Jr., W.W., Tuason, V.B., 1996. Magnetoencephalographic assessment of spontaneous brain activity in schizophrenia. Psychopharmacol. Bull. 32, 741–750.

Centers for Disease Control, Prevention, National Center for Injury Prevention, Control, 2003. Report to Congress on Mild Traumatic Brain Injury in the United States: Steps to Prevent a Serious Public Health Problem. Centers for Disease Control and Prevention, Atlanta, GA, USA.

Cernak, I., Noble-Haeusslein, L.J., 2010. Traumatic brain injury: an overview of pathobiology with emphasis on military populations. J. Cereb. Blood Flow Metab. 30, 255–266.

Cernak, I., Wang, Z., Jiang, J., Bian, X., Savic, J., 2001. Ultrastructural and functional characteristics of blast injury-induced neurotrauma. J. Trauma 50, 695–706.

Cohen, D., Schläpfer, U., Ahlfors, S., Hämäläinen, M., Halgren, E., 2002. New six-layer magnetically-shielded room for MEG. In: Nowak, H.H.J., Gießler, F. (Eds.), Proceedings of the 13th International Conference on Biomagnetism. VDE Verlag, Jena, Germany, pp. 919–921.

Culotta, V.P., Sementilli, M.E., Gerold, K., Watts, C.C., 1996. Clinicopathological heterogeneity in the classification of mild head injury. Neurosurgery 38, 245–250.

Davenport, N.D., Lim, K.O., Armstrong, M.T., Sponheim, S.R., 2012. Diffuse and spatially variable white matter disruptions are associated with blast-related mild traumatic brain injury. Neuroimage 59, 2017–2024.

de Jongh, A., Baayen, J.C., De Munck, J.C., Heethaar, R.M., Vandertop, W.P., Stam, C.J., 2003. The influence of brain tumor treatment on pathological delta activity in MEG. Neuroimage 20, 2291–2301.

Decker Jr., D.A., Knott, J.R., 1972. The EEG in intrinsic supratentorial brain tumors: a comparative evaluation. Electroencephalogr. Clin. Neurophysiol. 33, 303–310.

Dikmen, S.S., Ross, B.L., Machamer, J.E., Temkin, N.R., 1995. One year psychosocial outcome in head injury. J. Int. Neuropsychol. Soc. 1, 67–77.

Eiselt, H.A., Pederzoli, G., Sandblom, C.-L., 1987. Continuous Optimization Models. Walter de Gruyter, Berlin, New York.

Elder, G.A., Mitsis, E.M., Ahlers, S.T., Cristian, A., 2010. Blast-induced mild traumatic brain injury. Psychiatr. Clin. North Am. 33, 757–781.

Faul, M., Xu, L., Wald, M.M., Coronado, V.G., 2010. Traumatic brain injury in the United States: emergency department visits, hospitalizations, and deaths. Centers for Disease Control and Prevention, National Center for Injury Prevention and Control, Atlanta, GA, USA.

Fehr, T., Kissler, J., Moratti, S., Wienbruch, C., Rockstroh, B., Elbert, T., 2001. Source distribution of neuromagnetic slow waves and MEG-delta activity in schizophrenic patients. Biol. Psychiatry 50, 108–116.

Fehr, T., Kissler, J., Wienbruch, C., Moratti, S., Elbert, T., Watzl, H., Rockstroh, B., 2003. Source distribution of neuromagnetic slow-wave activity in schizophrenic patients—effects of activation. Schizophr. Res. 63, 63–71.

Fernandez, A., Maestu, F., Amo, C., Gil, P., Fehr, T., Wienbruch, C., Rockstroh, B., Elbert, T., Ortiz, T., 2002. Focal temporoparietal slow activity in Alzheimer's disease revealed by magnetoencephalography. Biol. Psychiatry 52, 764–770.

Fisch, B.J., 1999. Fisch and Spehlmann's EEG Primer: Basic Principles of Digital and Analog EEG. Elsevier.

Garman, R.H., Jenkins, L.W., Switzer III, R.C., Bauman, R.A., Tong, L.C., Swauger, P.V., Parks, S.A., Ritzel, D.V., Dixon, C.E., Clark, R.S., Bayir, H., Kagan, V., Jackson, E.K., Kochanek, P.M., 2011. Blast exposure in rats with body shielding is characterized primarily by diffuse axonal injury. J. Neurotrauma 28, 947–959.

Gennarelli, T.A., Thibault, L.E., Adams, J.H., Graham, D.I., Thompson, C.J., Marcincin, R.P., 1982. Diffuse axonal injury and traumatic coma in the primate. Ann. Neurol. 12, 564–574.

Gloor, P., Ball, G., Schaul, N., 1977. Brain lesions that produce delta waves in the EEG. Neurology 27, 326–333.

Green, P., 2005. Green's Word Memory Test (User's Manual). Green's Publishing Inc., Edmonton.

Gupta, R.K., Saksena, S., Agarwal, A., Hasan, K.M., Husain, M., Gupta, V., Narayana, P.A., 2005. Diffusion tensor imaging in late posttraumatic epilepsy. Epilepsia 46, 1465–1471.

Henry, L.C., Tremblay, J., Tremblay, S., Lee, A., Brun, C., Lepore, N., Theoret, H., Ellemberg, D., Lassonde, M., 2011. Acute and chronic changes in diffusivity measures after sports concussion. J. Neurotrauma 28, 2049–2059.

Huang, M.X., Aine, C., Davis, L., Butman, J., Christner, R., Weisend, M., Stephen, J., Meyer, J., Silveri, J., Herman, M., Lee, R.R., 2000. Sources on the anterior and posterior banks of the central sulcus identified from magnetic somatosensory evoked responses using multistart spatio-temporal localization. Hum. Brain Mapp. 11, 59–76.

Huang, M.X., Dale, A.M., Song, T., Halgren, E., Harrington, D.L., Podgorny, I., Canive, J.M., Lewis, S., Lee, R.R., 2006. Vector-based spatial-temporal minimum L1-norm solution for MEG. Neuroimage 31, 1025–1037.

Huang, M.X., Lee, R.R., Gaa, K.M., Song, T., Harrington, D.L., Loh, C., Theilmann, R.J., Edgar, J.C., Miller, G.A., Canive, J.M., Granholm, E., 2010. Somatosensory system deficits in schizophrenia revealed by MEG during a median-nerve oddball task. Brain Topogr. 23, 82–104.

Huang, M.X., Song, T., Hagler Jr., D.J., Podgorny, I., Jousmaki, V., Cui, L., Gaa, K., Harrington, D.L., Dale, A.M., Lee, R.R., Elman, J., Halgren, E., 2007. A novel integrated MEG and EEG analysis method for dipolar sources. Neuroimage 37, 731–748.

Huang, M.X., Theilmann, R.J., Robb, A., Angeles, A., Nichols, S., Drake, A., D'Andrea, J., Levy, M., Holland, M., Song, T., Ge, S., Hwang, E., Yoo, K., Cui, L., Baker, D.G., Trauner, D., Coimbra, R., Lee, R.R., 2009. Integrated imaging approach with MEG and DTI to detect mild traumatic brain injury in military and civilian patients. J. Neurotrauma 26, 1213–1226.

Huisman, T.A., Schwamm, L.H., Schaefer, P.W., Koroshetz, W.J., Shetty-Alva, N., Ozsunar, Y., Wu, O., Sorensen, A.G., 2004. Diffusion tensor imaging as potential biomarker of white matter injury in diffuse axonal injury. AJNR Am. J. Neuroradiol. 25, 370–376.

Inglese, M., Makani, S., Johnson, G., Cohen, B.A., Silver, J.A., Gonen, O., Grossman, R.I., 2005. Diffuse axonal injury in mild traumatic brain injury: a diffusion tensor imaging study. J. Neurosurg. 103, 298–303.

Ioannides, A.A., Singh, K.D., Hasson, R., Baumann, S.B., Rogers, R.L., Guinto Jr., F.C., Papanicolaou, A.C., 1993. Comparison of single current dipole and magnetic field tomography analyses of the cortical response to auditory stimuli. Brain Topogr. 6, 27–34.

Johnston, K.M., Ptito, A., Chankowsky, J., Chen, J.K., 2001. New frontiers in diagnostic imaging in concussive head injury. Clin. J. Sport Med. 11, 166–175.

Kirkwood, M.W., Yeates, K.O., Wilson, P.E., 2006. Pediatric sport-related concussion: a review of the clinical management of an oft-neglected population. Pediatrics 117, 1359–1371.

Lee, J.W., Choi, C.G., Chun, M.H., 2006. Usefulness of diffusion tensor imaging for evaluation of motor function in patients with traumatic brain injury: three case studies. J. Head Trauma Rehabil. 21, 272–278.

Leung, L.Y., VandeVord, P.J., Dal Cengio, A.L., Bir, C., Yang, K.H., King, A.I., 2008. Blast related neurotrauma: a review of cellular injury. Mol. Cell. Biomech. 5, 155–168.

Levin, H.S., Amparo, E., Eisenberg, H.M., Williams, D.H., High Jr., W.M., McArdle, C.B., Weiner, R.L., 1987. Magnetic resonance imaging and computerized tomography in relation to the neurobehavioral sequelae of mild and moderate head injuries. J. Neurosurg. 66, 706–713.

Levy, M.L., Ozgur, B.M., Berry, C., Aryan, H.E., Apuzzo, M.L., 2004. Birth and evolution of the football helmet. Neurosurgery 55, 656–661.

Lewine, J.D., Davis, J.T., Bigler, E.D., Thoma, R., Hill, D., Funke, M., Sloan, J.H., Hall, S., Orrison, W.W., 2007. Objective documentation of traumatic brain injury subsequent to mild head trauma: multimodal brain imaging with MEG, SPECT, and MRI. J. Head Trauma Rehabil. 22, 141–155.

Lewine, J.D., Davis, J.T., Sloan, J.H., Kodituwakku, P.W., Orrison Jr., W.W., 1999. Neuromagnetic assessment of pathophysiologic brain activity induced by minor head trauma. AJNR Am. J. Neuroradiol. 20, 857–866.

Lewine, J.D., Orrison Jr., W.W., 1995. Spike and slow wave localization by magnetoencephalography. Neuroimaging Clin. N. Am. 5, 575–596.

Mac Donald, C.L., Johnson, A.M., Cooper, D., Nelson, E.C., Werner, N.J., Shimony, J.S., Snyder, A.Z., Raichle, M.E., Witherow, J.R., Fang, R., Flaherty, S.F., Brody, D.L., 2011. Detection of blast-related traumatic brain injury in U.S. military personnel. N. Engl. J. Med. 364, 2091–2100.

MacGregor, A.J., Dougherty, A.L., Galarneau, M.R., 2010. Injury-specific correlates of combat-related traumatic brain injury in operation iraqi freedom. J. Head Trauma Rehabil. 25, 1–8.

Matsuura, K., Okabe, Y., 1997. A robust reconstruction of sparse biomagnetic sources. IEEE Trans. Biomed. Eng. 44, 720–726.

Mayer, A.R., Mannell, M.V., Ling, J., Gasparovic, C., Yeo, R.A., 2011. Functional connectivity in mild traumatic brain injury. Hum. Brain Mapp. 32, 1825–1835.

McLean Jr., A., Dikmen, S., Temkin, N., Wyler, A.R., Gale, J.L., 1984. Psychosocial functioning at 1 month after head injury. Neurosurgery 14, 393–399.

Messe, A., Caplain, S., Paradot, G., Garrigue, D., Mineo, J.F., Soto, A.G., Ducreux, D., Vignaud, F., Rozec, G., Desal, H., Pelegrini-Issac, M., Montreuil, M., Benali, H., Lehericy, S., 2011. Diffusion tensor imaging and white matter lesions at the subacute stage in mild traumatic brain injury with persistent neurobehavioral impairment. Hum. Brain Mapp. 32, 999–1011.

Miles, L., Grossman, R.I., Johnson, G., Babb, J.S., Diller, L., Inglese, M., 2008. Short-term DTI predictors of cognitive dysfunction in mild traumatic brain injury. Brain Inj. 22, 115–122.

Mosher, J.C., Leahy, R.M., Lewis, P.S., 1999. EEG and MEG: forward solutions for inverse methods. IEEE Trans. Biomed. Eng. 46, 245–259.

Moss, W.C., King, M.J., Blackman, E.G., 2009. Skull flexure from blast waves: a mechanism for brain injury with implications for helmet design. Phys. Rev. Lett. 103, 108702.

Nagata, K., Gross, C.E., Kindt, G.W., Geier, J.M., Adey, G.R., 1985. Topographic electroencephalographic study with power ratio index mapping in patients with malignant brain tumors. Neurosurgery 17, 613–619.

Niedermeyer, E., Da, F.D., 2005. Electroencephalography: Basic Principles, Clinical Applications, and Related Fields, 5th ed. Lippincott Williams & Wilkins, Philadelphia, Baltimore, New York, London, Buenos Aires, Hong Kong, Sydney, Tokyo.

Niogi, S.N., Mukherjee, P., Ghajar, J., Johnson, C., Kolster, R.A., Sarkar, R., Lee, H., Meeker, M., Zimmerman, R.D., Manley, G.T., McCandliss, B.D., 2008. Extent of microstructural white matter injury in postconcussive syndrome correlates with impaired cognitive reaction time: a 3T diffusion tensor imaging study of mild traumatic brain injury. AJNR Am. J. Neuroradiol. 29, 967–973.

Nyein, M.K., Jason, A.M., Yu, L., Pita, C.M., Joannopoulos, J.D., Moore, D.F., Radovitzky, R.A., 2010. In silico investigation of intracranial blast mitigation with relevance to military traumatic brain injury. Proc. Natl. Acad. Sci. U. S. A. 107, 20703–20708.

Okie, S., 2005. Traumatic brain injury in the war zone. N. Engl. J. Med. 352, 2043–2047.

Rimel, R.W., Giordani, B., Barth, J.T., Boll, T.J., Jane, J.A., 1981. Disability caused by minor head injury. Neurosurgery 9, 221–228.

Rockstroh, B.S., Wienbruch, C., Ray, W.J., Elbert, T., 2007. Abnormal oscillatory brain dynamics in schizophrenia: a sign of deviant communication in neural network? BMC Psychiatry 7, 44.

Rowan, A.J., Tolunsky, E., 2003. Primer of EEG with a Mini-Atlas. Butterworth Heinemann.

Rutgers, D.R., Toulgoat, F., Cazejust, J., Fillard, P., Lasjaunias, P., Ducreux, D., 2008. White matter abnormalities in mild traumatic brain injury: a diffusion tensor imaging study. AJNR Am. J. Neuroradiol. 29, 514–519.

Rutherford, W.H., 1989. Postconcussion symptoms: relationship to acuteneurological indices, individual differences, and circumstances of injury. In: Levin, H., Eisenberg, H., Benton, A.L. (Eds.), Mild Head Injury. Oxford University Press, New York, pp. 217–228.

Salmond, C.H., Menon, D.K., Chatfield, D.A., Williams, G.B., Pena, A., Sahakian, B.J., Pickard, J.D., 2006. Diffusion tensor imaging in chronic head injury survivors: correlations with learning and memory indices. Neuroimage 29, 117–124.

Schaul, N., Gloor, P., Ball, G., Gotman, J., 1978. The electromicrophysiology of delta waves induced by systemic atropine. Brain Res. 143, 475–486.

Smits, M., Houston, G.C., Dippel, D.W., Wielopolski, P.A., Vernooij, M.W., Koudstaal, P.J., Hunink, M.G., van der,, L.A., 2011. Microstructural brain injury in post-concussion syndrome after minor head injury. Neuroradiology 53, 553–563.

Song, T., Gaa, K., Cui, L., Feffer, L., Lee, R.R., Huang, M., 2008. Evaluation of signal space separation via simulation. Med. Biol. Eng. Comput. 46, 923–932.

Taulu, S., Kajola, M., Simola, J., 2004a. Suppression of interference and artifacts by the signal space separation method. Brain Topogr. 16, 269–275.

Taulu, S., Simola, J., Kajola, M., 2004b. MEG recordings of DC fields using the signal space separation method (SSS). Neurol. Clin. Neurophysiol. 2004, 35.

Teasdale, G., Jennett, B., 1974. Assessment of coma and impaired consciousness. A practical scale. Lancet 2, 81–84.

Thurman, D.J., Alverson, C., Dunn, K.A., Guerrero, J., Sniezek, J.E., 1999. Traumatic brain injury in the United States: a public health perspective. J. Head Trauma Rehabil. 14, 602–615.

Uutela, K., Hamalainen, M., Somersalo, E., 1999. Visualization of magnetoencephalographic data using minimum current estimates. Neuroimage 10, 173–180.

Van Boven, R.W., Harrington, G.S., Hackney, D.B., Ebel, A., Gauger, G., Bremner, J.D., D'Esposito, M., Detre, J.A., Haacke, E.M., Jack Jr., C.R., Jagust, W.J., Le, B.D., Mathis, C.A., Mueller, S., Mukherjee, P., Schuff, N., Chen, A., Weiner, M.W., 2009. Advances in neuroimaging of traumatic brain injury and posttraumatic stress disorder. J. Rehabil. Res. Dev. 46, 717–757.

Vieth, J.B., Kober, H., Grummich, P., 1996. Sources of spontaneous slow waves associated with brain lesions, localized by using the MEG. Brain Topogr. 8, 215–221.

Wilde, E.A., Chu, Z., Bigler, E.D., Hunter, J.V., Fearing, M.A., Hanten, G., Newsome, M.R., Scheibel, R.S., Li, X., Levin, H.S., 2006. Diffusion tensor imaging in the corpus callosum in children after moderate to severe traumatic brain injury. J. Neurotrauma 23, 1412–1426.

Wilde, E.A., McCauley, S.R., Hunter, J.V., Bigler, E.D., Chu, Z., Wang, Z.J., Hanten, G.R., Troyanskaya, M., Yallampalli, R., Li, X., Chia, J., Levin, H.S., 2008. Diffusion tensor imaging of acute mild traumatic brain injury in adolescents. Neurology 70, 948–955.

Xu, J., Rasmussen, I.A., Lagopoulos, J., Haberg, A., 2007. Diffuse axonal injury in severe traumatic brain injury visualized using high-resolution diffusion tensor imaging. J. Neurotrauma 24, 753–765.

Zhang, K., Johnson, B., Pennell, D., Ray, W., Sebastianelli, W., Slobounov, S., 2010. Are functional deficits in concussed individuals consistent with white matter structural alterations: combined FMRI & DTI study. Exp. Brain Res. 204, 57–70.